CDC-42 and RAC-1 regulate opposite chemotropisms in Neurospora crassa

© 2014. Published by The Company of Biologists Ltd | Journal of Cell Science (2014) 127, 1953–1965 doi:10.1242/jcs.141630

RESEARCH ARTICLE

CDC-42 and RAC-1 regulate opposite chemotropisms in *Neurospora crassa*

Alexander Lichius[1,2,*], Andrew B. Goryachev[1], Mark D. Fricker[3], Boguslaw Obara[4], Ernestina Castro-Longoria[2] and Nick D. Read[1,*]

ABSTRACT

Cell polarization and fusion are crucial developmental processes that occur in response to intracellular and extracellular signals. Asexual spores (conidia) of the mold *Neurospora crassa* differentiate two types of polarized cell protrusions, germ tubes and conidial anastomosis tubes (CATs), which exhibit negative and positive chemotropism, respectively. We provide the first evidence that shared and separate functions of the Rho-type GTPases CDC-42 and RAC-1 regulate these opposite chemotropisms. We demonstrate that RAC-1 is essential for CAT formation and cell fusion, whereas CDC-42 is necessary and sufficient for normal germ tube development. Cdc42-Rac-interactive-binding (CRIB) reporters were constructed to exclusively label locally activated GTP-bound GTPases. Time course analyses showed that repositioning of these activated GTPase clusters within germ tube and CAT tip apices controls directional growth in the absence of a tip-localized vesicle supply center (Spitzenkörper). We propose a model in which the local assembly of a plasma-membrane-associated GTPase–PAK–MAPK signaling platform regulates chemoattractant perception and secretion in order to synchronize oscillatory cell–cell communication and directional CAT tip growth.

KEY WORDS: CDC-42, RAC-1, CRIB, Conidial anastomosis tube, *Neurospora crassa*, Cell fusion, Chemotropism, Directional tip growth

INTRODUCTION

Cell polarization is a crucial developmental process that occurs in response to distinct intracellular and extracellular cues, including cortical landmarks, nutrient gradients, pheromones and other tropic signals. The small Rho-type GTPases Cdc42 and Rac1 are key regulators of eukaryotic cell polarity (Jaffe and Hall, 2005; Virag et al., 2007). They switch between inactive GDP-bound and active GTP-bound states, and this switching is tightly controlled *in vivo* by guanine nucleotide exchange factors (GEFs) (Schmidt and Hall, 2002) and GTPase-activating proteins (GAPs) (Bernards and Settleman, 2004). Nucleotide cycling of Rho GTPases is coupled to their membrane–cytoplasmic shuttling mediated by guanine nucleotide dissociation inhibitors (GDIs) (Seabra and Wasmeier, 2004). The key outcome of this is that GTPase activity becomes amplified and focused at specific locations at the cell cortex (Goryachev and Pokhilko, 2008). Activated GTPases act on multiple effector molecules, such as p21-activated kinases (PAKs) and mitogen-activated protein kinases (MAPKs), which regulate numerous cellular processes (Bishop and Hall, 2000), including remodeling of the actin cytoskeleton and targeted secretion of cell wall precursors that initiate polarized protrusion of the cell cortex (Nelson, 2003).

Filamentous fungi are well-established models for studying polarized cell growth in response to tropic cues (Brand and Gow, 2009). In the unicellular fungi *Saccharomyces cerevisiae* and *Schizosaccharomyces pombe*, Cdc42 alone is necessary and sufficient to control polarized growth (Adams et al., 1990; Miller and Johnson, 1994). Significantly, orthologs of the other crucial GTPase, Rac1, are absent from these yeast genomes. In contrast, multicellular filamentous fungi require both Rho GTPases to regulate their greater morphogenetic prowess, including much faster tip growth and the ability to maintain multiple axes of polarity. Although Cdc42 and Rac1 are structurally very similar (they have 59% amino acid sequence identity in *Neurospora crassa*) and highly conserved across fungal species, increasing evidence suggests that their biological functions differ significantly (Mahlert et al., 2006; Virag et al., 2007). Functionally diverse signaling of GTPases is regulated through selective interaction with GDIs, GEFs and GAPs (Jaffe and Hall, 2005). Key determinants of selectivity of Cdc42 and Rac1 for their cognate GEFs is conferred through specific residues in the GEF-binding domains of both GTPases. A tryptophan or tyrosine residue at position 56 is specific for CDC-42, whereas a phenylalanine residue at position 56 and an alanine residue at position 27 are specific for Rac (Gao et al., 2001; Karnoub et al., 2001; Kulkarni et al., 2011). Recent studies on the filamentous fungus *N. crassa* identified an important role for CDC-42 in initiating cell polarity, whereas RAC-1 was predominantly involved in the maintenance of polarized tip growth (Araujo-Palomares et al., 2011). The CDC-24 GEF is equally effective at regulating both GTPases *in vitro*, suggesting that the specificities of both GTPases lie downstream, most likely via specific effector protein interactions. However, which cellular processes are controlled by these two GTPases mutually and which rely on their differing activities is still poorly understood in any eukaryotic system. Here, using *N. crassa* as a model organism, we identify different functions of these GTPases in processes controlling cellular polarization and chemotropism.

Two PAKs, orthologous to Ste20 and Cla4 from *S. cerevisiae*, are encoded in filamentous fungal genomes. However, we know

[1]Institute of Cell Biology, University of Edinburgh, Mayfield Road, Edinburgh EH9 3JR, Scotland, UK. [2]Department of Microbiology, Center for Scientific Research and Higher Education of Ensenada (CICESE), Carretera Ensenada-Tijuana 3918, 22860 Ensenada, Baja California, México. [3]Department of Plant Sciences, University of Oxford, South Park Road, Oxford OX1 3RB, UK. [4]School of Engineering and Computing Sciences, Durham University, South Road, Durham DH1 3LE, UK.

*Authors for correspondence (alexander.lichius@tuwien.ac.at; Nick.Read@manchester.ac.uk)

Received 29 August 2013; Accepted 13 January 2014

Journal of Cell Science (2014) 127, 1953–1965 doi:10.1242/jcs.141630

very little about their role in cell fusion in *N. crassa*. Recently, we have shown that F-actin is important during germ tube and conidial anastomosis tube (CAT) growth (Berepiki et al., 2010), whereas microtubules are only essential for germ tube elongation (Roca et al., 2010b). Based on these findings, we first hypothesize that apically focused Rho GTPase activity plays a key role in the spatio-temporal coordination of F-actin remodeling in response to MAK-2-dependent signaling, controlling CAT chemoattraction prior to cell fusion, and that this might involve the PAKs CLA-4 or STE-20 as key GTPase effectors. Activated PAKs, in turn, act on MAPKs to trigger specific signaling cascades for cell–cell communication, directional tip growth and cell wall remodeling.

Neurospora crassa possesses three distinct MAPK cascade modules, resembling the pheromone response, cell wall integrity (CWI) and high osmolarity glycerol (HOG) pathways of *S. cerevisiae* (Lengeler et al., 2000; Borkovich et al., 2004; Chen and Thorner, 2007). MAPKs of the pheromone response (PR) and CWI pathways, but not the HOG pathway, are required for cell fusion in *N. crassa* (Pandey et al., 2004; Li et al., 2005; Roca et al., 2005; Maerz et al., 2008; Lichius et al., 2012a). The PR pathway MAPK MAK-2 exhibits oscillatory recruitment to CAT tips as they grow chemotropically towards each other. It plays a key role in the 'ping pong' mechanism, which repeatedly switches the physiological states of two interacting, genetically identical cells for them to recognize each other as different and fuse (Fleissner et al., 2009; Read et al., 2012).

Germ tubes generally exhibit negative chemotropisms towards each other (germ tube avoidance) whereas CATs undergo positive chemotropisms towards other CATs (CAT homing). It is not known how these opposite chemotropic responses from the same cell are regulated. Mutants defective in CAT formation do not seem to inhibit germ tube avoidance (Fig. 1), suggesting that each chemotropic response is controlled by a separate signaling mechanism. Our second hypothesis, therefore, is that the CDC-42 and RAC-1 GTPases have distinct roles in the formation and chemotropic behavior of germ tubes and CATs, respectively.

The Spitzenkörper, which plays a role as a vesicle supply center, is instrumental in controlling directional tip growth in mature hyphal tips (Bartnicki-Garcia et al., 1995; Lopez-Franco and Bracker, 1996). A similar structure, however, has so far not been recognized in germ tube tips of *Neurospora* that are less than 150 µm in length (Araujo-Palomares et al., 2007) or in CATs (Roca et al., 2005), raising the question as to how directional changes during germ tube avoidance and CAT homing are realized in the absence of a Spitzenkörper. Thus, our third hypothesis is that activated GTPases are central components of a plasma-membrane-associated cortical vesicle supply center that organizes targeted secretion during directional tip growth of germ tubes and CATs in response to chemotropic cues.

To test these three hypotheses, we have compared the morphology and development of *N. crassa* GTPase and PAK deletion mutants, and determined the localization patterns of fluorescently labeled CDC-42 and RAC-1 in conidial germlings.

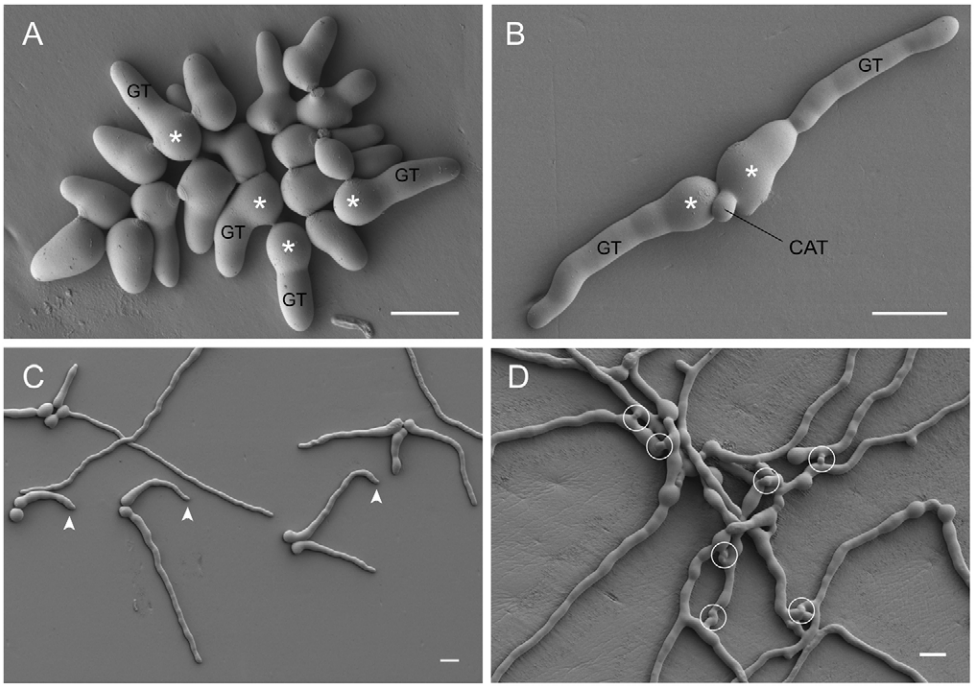

Fig. 1. Opposite chemotropic behavior of germ tubes and CATs. Low-temperature scanning electron micrographs of conidial germlings of *N. crassa*. (A) In cell groups, germ tubes (GT) exhibit a strong tendency to emerge from the spore body (asterisk) in a way such that they keep a maximal distance away from neighboring cells or germ tubes. This shows that already during cell symmetry breaking, the presence of other cells has been sensed and germ tube avoidance appropriately controlled. (B) CATs, by contrast, will often emerge from positions where the cell cortex is closest to neighboring cells. (C) In close proximity to other germ tubes, germ tubes will redirect their tip growth direction before physical contact can occur (avoiding tips are indicated by arrowheads), confirming that diffusible molecules must act as chemorepellants. (D) Positive chemotropism of CATs is instrumental for the formation of an interconnected, supracellular germling network (cell fusion connections are circled). A and C show the Δ*mak-2* gene deletion mutant defective in CAT formation, whereas B and D show the wild type. Avoidance responses of the mutant show that a CAT formation and/or fusion defect does not necessarily interfere with negative chemotropism of germ tubes, suggesting that both chemotropic responses are controlled by separate signaling pathways. Scale bars: 10 µm.

Journal of Cell Science (2014) 127, 1953–1965 doi:10.1242/jcs.141630

To selectively analyze the spatio-temporal dynamics of locally activated CDC-42 and RAC-1 during germ tube and CAT development, we have generated Cdc42-Rac-interactive-binding (CRIB) reporters for *N. crassa* along with custom-designed automated tip-tracking image analysis software. Furthermore, we have conducted pharmacological studies to selectively inhibit RAC-1 activity in order to discriminate between CDC-42 and RAC-1 functions.

RESULTS

Deletion phenotypes of CDC-42 and RAC-1 suggest functional divergence between the two

Deletion mutants of *N. crassa* CDC-42 and RAC-1 have severe polarity defects during vegetative hyphal growth (Araujo-Palomares et al., 2011). Here, we show that the absence of these proteins also affects cell fusion; CAT formation was completely blocked in both Δ*cdc-42* and Δ*rac-1* germlings (Fig. 2A–C) and hyphal fusion was absent in the mature colonies (Fig. 2D–F). Because hyphal differentiation was greatly impaired in each strain, it was not possible to distinguish morphologically distinct fusion hyphae (Hickey et al., 2002) from other hyphae in the mycelium. Nevertheless, the Δ*cdc-42* and Δ*rac-1* mutants displayed clearly distinct growth phenotypes. Whereas Δ*rac-1* cells managed to initiate and maintain polarized growth of elongated germ tubes and mature hyphae (Fig. 2C,F), the Δ*cdc-42* mutant was unable to set and maintain a fixed polar axis, leading to extended isotropic growth and greatly impaired hyphal elongation (Fig. 2B,E). We infer that the more general role of CDC-42 in establishing polarized growth explains the lack of normal germ tubes and CATs in Δ*cdc-42* germlings, whereas a more specific role of RAC-1 during germling development is responsible for the absence of CATs in Δ*rac-1* only. Consequently, this suggests that the two GTPases are not functionally interchangeable, and CDC-42 is sufficient to support germ tube formation in Δ*rac-1*, whereas RAC-1 is insufficient for CAT formation in Δ*cdc-42*. Because of the known functional link between the two Rho GTPases and their putative downstream effector PAKs (Jaffe and Hall, 2005), we analyzed the fusion phenotype of *N. crassa* CLA-4 and STE-20 gene deletion mutants (Fig. 3). Strikingly, the Δ*cla-4*, but not the Δ*ste-20* mutant, showed phenotypic defects associated with cell fusion, indicating that only CLA-4 has an important role in this process. The Δ*cla-4* phenotype partly resembled that of Δ*rac-1*, including no CAT formation, dichotomous branching and extremely dense colony development. However with time, germling and hyphal fusion connections were established in the mutant, although with greatly altered morphology (Fig. 3C,E).

CDC-42 and RAC-1 show indistinguishable subcellular localization in conidial germlings

In mature hyphal tips, CDC-42 and RAC-1 are spatially separated: CDC-42 localizes to a confined crescent at the very apex, whereas RAC-1 forms an apical ring outside of the region occupied by CDC-42 (Araujo-Palomares et al., 2011). To determine whether putative functional differences between the two GTPases result in different cortical localizations in germ tubes and CATs, we compared the subcellular localization patterns of fluorescently tagged CDC-42 and RAC-1 in conidial germlings. In line with previous findings (Araujo-Palomares et al., 2011), apical crescents of CDC-42 and RAC-1 were constantly present in the tips of growing germ tubes (Fig. 2G,H), and in homing and fusing CAT tips (Fig. 2I,J). In addition, both GTPases accumulated in circular internal membrane structures (arrows in Fig. 2G,H). Identical labeling patterns have been observed with the perinuclear endoplasmic reticulum (ER) marker BEM-46 (Mercker et al., 2009), indicating that both GTPases might localize to this compartment. Upon CAT contact, GTPase fluorescence intensified at the incipient fusion site (arrows in Fig. 2I,J), then disappeared shortly after fusion was completed. Thus, the similar localization patterns of CDC-42 and RAC-1 in germlings were notably different from that observed in mature hyphal tips.

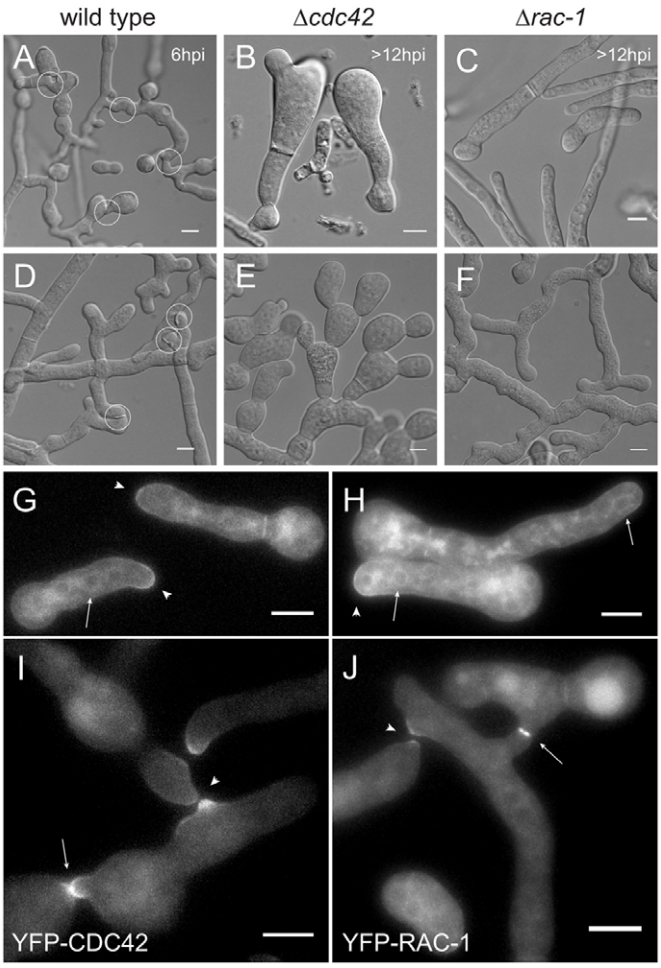

Fig. 2. Deletion of *cdc-42* or *rac-1* severely affects germling morphogenesis, and inhibits cell fusion. (A) Wild-type conidial germlings form supracellular networks by CAT-mediated cell fusion within 6 h of incubation (fusion connections are indicated with circles). (B) Δ*cdc-42* conidial germlings lack CATs and elongated germ tubes, and display extremely slow, but increased isotropic expansion. (C) In Δ*rac-1* germlings, germ tube growth is much less severely affected compared to Δ*cdc-42*; CATs, however, are also not formed. (D) Specialized fusion hyphae establish the interconnected hyphal network in the mature colony of the wild type. (E) Mature hyphae of Δ*cdc-42* exhibit increased isotropic expansion, dichotomous branching, lack hyphal differentiation and do not undergo hyphal fusion. (F) Mature hyphae of Δ*rac-1* are elongated but cannot fuse. (G,H) YFP–CDC-42 and YFP–RAC-1 show indistinguishable labeling patterns in germ tubes, accumulating as apical crescents at growing tips (arrowheads), at forming septa and also within intracellular membrane compartments that appear to be the nuclear envelope and possibly the perinuclear ER (circular structures; some indicated with arrows). (I,J) Both GTPases show identical localization patterns in homing CAT tips (arrowheads) and at sites of cell fusion (arrows). hpi, hours post inoculation. Scale bars: 10 μm (A–F); 5 μm (G–J).

Journal of Cell Science (2014) 127, 1953–1965 doi:10.1242/jcs.141630

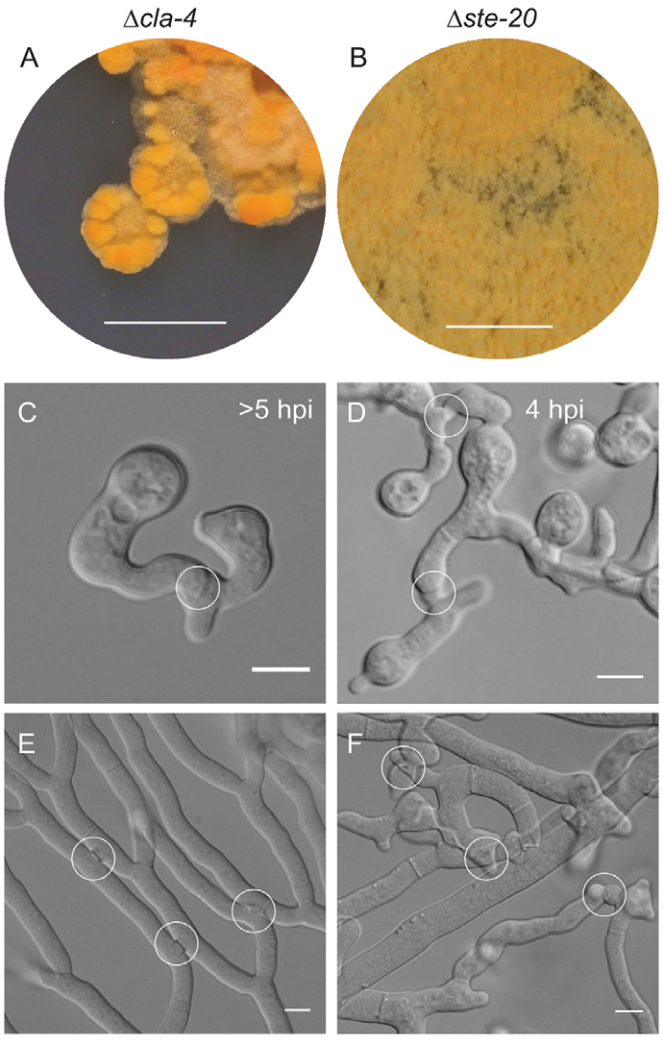

Fig. 3. Polarity and cell fusion defects in PAK gene deletion mutants Δ*cla-4* and Δ*ste-20*. (A) Deletion of CLA-4 (Δ*cla-4*) caused severe polarity defects, leading to developmental delays (radial extension reduced to <2 mm/day compared to wild type with >45 mm/day) and extremely dense growing colonies, reminiscent of the Δ*rac-1* colony phenotype (Araujo-Palomares et al., 2011). (B) In contrast, deletion of STE-20, the second PAK of *N. crassa* (Δ*ste-20*), caused no obvious mutant phenotype. Colony morphologies in A and B were recorded after 3 days of incubation at 30°C on VMM. Scale bars: 10 mm. (C,D) Despite a significant developmental delay (onset of CAT fusion in Δ*cla-4* was on average 2–3 h later than the wild type), conidial germlings of Δ*cla-4* (C) were able to fuse (shown in circles), although CATs were not clearly distinguishable. In contrast, conidial germlings of Δ*ste-20* formed germling networks by CAT fusion (D) that were morphologically indistinguishable from the wild type. hpi, hours post inoculation. (E,F) Mature hyphae after 2–4 days of incubation at 30°C on VMM. The Δ*cla-4* mutant (E) displayed a strictly dichotomous branching pattern and lacked clear hyphal differentiation but underwent lateral fusion between adjacent hyphae (circled). Mycelial development including the formation of functional fusion hyphae in the Δ*ste-20* strain (F) was indistinguishable from the wild-type morphology. Scale bars: 10 μm.

CRIB reporters colocalize with F-actin and sterol-rich plasma membrane regions during cell cortex polarization

To differentiate between populations of inactive GDP-bound and active GTP-bound GTPases, we generated Cdc42-CRIB reporters for *N. crassa* (Fig. 4). For this, we identified the CRIB motif within the p21-binding domain (PBD) of the two *N. crassa* PAKs STE-20 and CLA-4 by alignment with the eukaryotic CRIB consensus sequence (Bishop and Hall, 2000; Hoffman and Cerione, 2000) (Fig. 4A). We then subcloned gene regions encoding the PBD plus the associated pleckstrin homology (PH) or basic rich (BR) membrane-interaction domains of CLA-4 and STE-20, respectively, and fused them to GFP or TagRFP-T (Fig. 4B). Although the labeling patterns of all three CRIB reporters were identical (Fig. 4C), and their expression did not adversely impact colony morphology or hyphal extension rates (supplementary material Fig. S1), the $CRIB^{CLA-4}$–GFP construct was used for all further investigations presented in this paper owing to its superior signal-to-noise ratio and reliably consistent expression. Functionality of a minimal, synthetic CRIB reporter (sCRIB–GFP), comprising only the CRIB domain, was assessed too, but it only displayed cytoplasmic localization without specific recruitment properties. This confirmed the importance of both plasma-membrane-interaction domains for functional localization of PAKs leading to GTPase activation (Takahashi and Pryciak, 2007) (Fig. 4B,C).

In ungerminated non-polarized cells, CRIB reporter fluorescence was exclusively cytoplasmic (Fig. 5A). Initiation and maintenance of polarized growth coincided with the recruitment of the reporter into cortical crescents (Fig. 5B), indicating that GTPases became locally activated at polarization sites. The apical crescents of the CRIB reporter remained associated with growing germ tube tips (Fig. 5C) and CATs, but disappeared rapidly when polarized growth ceased upon the successful completion of CAT fusion (Fig. 5D; supplementary material Movie 1). Colocalization of the CRIB reporter with Lifeact-TagRFP-T, confirmed the close spatio-temporal relationship between GTPase activity and remodeling of the actin cytoskeleton at germ tube and CAT tips, and at cell fusion sites (Fig. 5E,F). Filipin staining was used to highlight sterol-rich plasma membrane regions, which have been shown to correlate with sites of increased exocytosis during cell cortex polarization (Takeshita et al., 2008). Filipin staining patterns during cell symmetry breaking (Fig. 5G), polarized tip protrusion (Fig. 5H,I) and CAT fusion (Fig. 5J) were similar to that of the CRIB reporter, which was verified by colocalization of both polarity markers (Fig. 5K). Taken together, our results are consistent with localized activation of GTPases initiating the polymerization of F-actin cable tracks to guide targeted vesicle secretion for polarized cell cortex protrusion in conidial germlings of *N. crassa*. Comparison of the CRIB reporter labeling patterns (Fig. 5B–E,K) with that of the YFP-labeled GTPases (Fig. 2G–J) further suggests that intracellular localization of the full-length GTPases most likely represents inactive GDP-bound populations of CDC-42 and RAC-1. Lack of intracellular localization might also be attributed to the fact that some sites, such as the nuclear envelope or perinuclear ER, might not be accessible to the CRIB reporter.

Repositioning of apical GTPase activity regulates growth directionality

Next, we addressed whether cortical recruitment and lateral repositioning of activated GTPases within the cell tip regulates directional chemotropic growth in germ tubes and CATs. During germ tube avoidance responses the apical crescent of CRIB reporter fluorescence translocated away from the opposing tip (Fig. 6A; supplementary material Movie 2). Conversely, during CAT homing, the peak CRIB fluorescence shifted towards the other tip and became focused at the incipient fusion site (Fig. 6B; supplementary material Movie 3). In both cases of chemotropism, repositioning of the CRIB reporter signal relative to the tip center

Journal of Cell Science (2014) 127, 1953–1965 doi:10.1242/jcs.141630

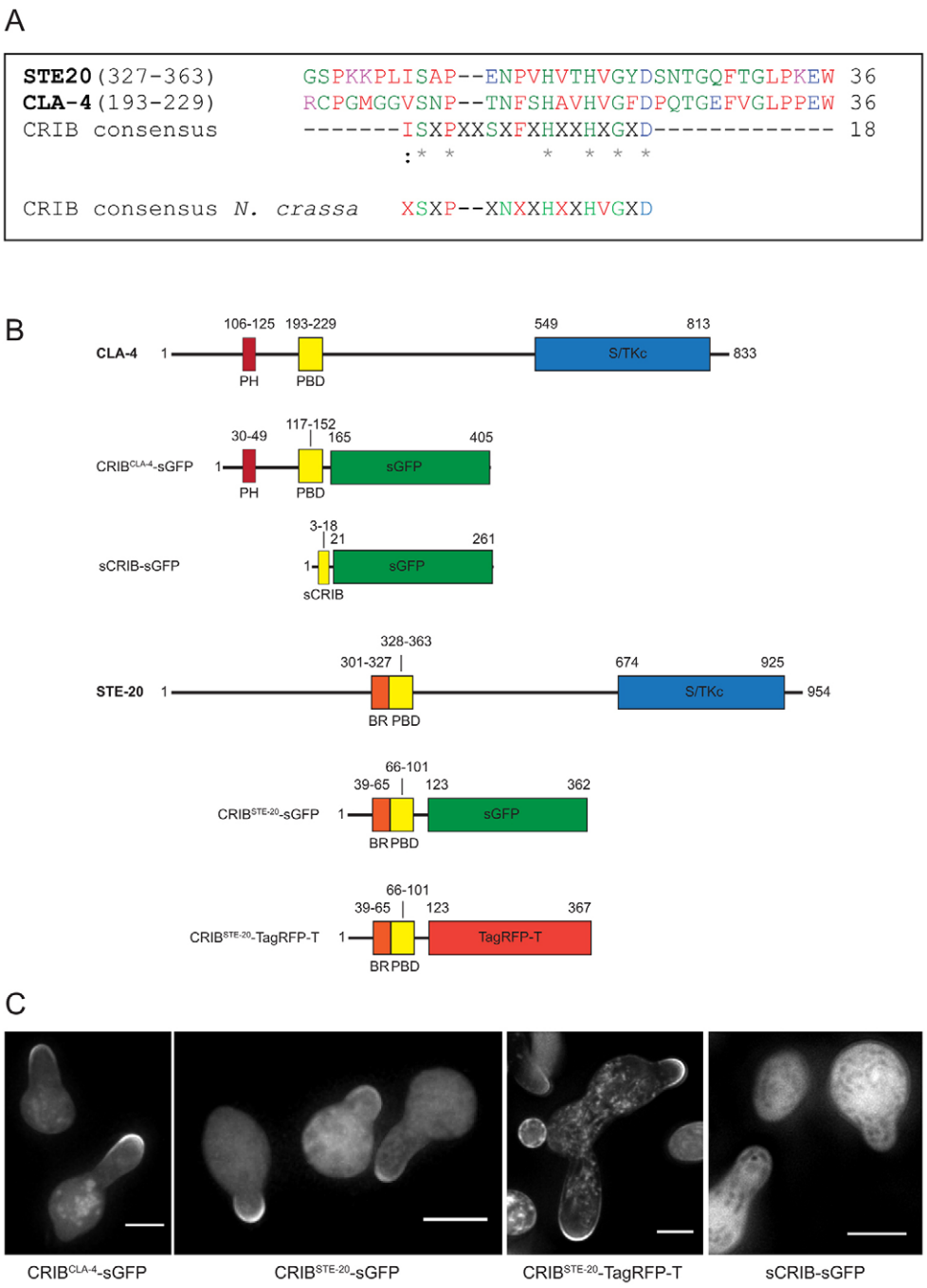

Fig. 4. Construction of CRIB reporters for *N. crassa*. (A) The *N. crassa* genome encodes two PAKs: STE-20 (NCU03894.2) and CLA-4 (NCU00406.2). The CRIB motif within the p21-binding domain (PBD) of each PAK was identified by alignment with the eukaryotic CRIB consensus sequence (Bishop and Hall, 2000; Hoffman and Cerione, 2000). Red, small or hydrophobic amino acids; blue, acidic amino acids; magenta, basic amino acids; green, hydroxyl amine amino acids. (B) Each PAK of *Neurospora* contains a PBD and a catalytic serine/threonine kinase (S/TKc) domain, as well as additional domains required for plasma membrane-localized activation of the kinase. CLA-4 utilizes a pleckstrin homology (PH) domain, whereas STE-20 contains a basic-rich (BR) domain. Numbers denote amino acid positions at the beginning and end of conserved domains, respectively. Both, BR and PH domains are essential for functional localization of PAKs, and activation of GTPases at the cell cortex. The BR domain of Ste20 can functionally substitute for the loss of the PH domain of Cla4 in *S. cerevisiae* (Takahashi and Pryciak, 2007). A synthetic CRIB construct (sCRIB–GFP), only comprising the CRIB motif (underlined in the following amino acid sequence) plus two adjoining amino acids on either side (GGVSNPTNFSHAVHVGFDPQ), and therefore lacking the associated PH domain, was insufficient for the labeling of activated GTPases (see C). In order to test the influence of the fluorescent protein label on subcellular localization of the reporter construct, and to facilitate future co-expression with CRIB^{CLA-4}, CRIB^{STE-20} was tagged with the red fluorescent protein TagRFP-T. (C) All three 'full-length' CRIB reporters containing the PBD and PH or BR domains, respectively, consistently localized to sites of polarized growth, whereas the synthetic CRIB reporter (sCRIB–GFP) only showed cytoplasmic localization. Notably, the TagRFP-T tag also resulted in elevated vacuolar background fluorescence, probably due to the generally higher stability of RFPs at low pH (Lichius and Read, 2010). Nevertheless, the basic labeling pattern of all three full-length CRIB reporters was identical, demonstrating robust functionality of all constructs. Owing to its superior signal-to-noise ratio and consistent expression, the CRIB^{CLA-4}–GFP construct was used for all investigations presented in this paper.

Journal of Cell Science (2014) 127, 1953–1965 doi:10.1242/jcs.141630

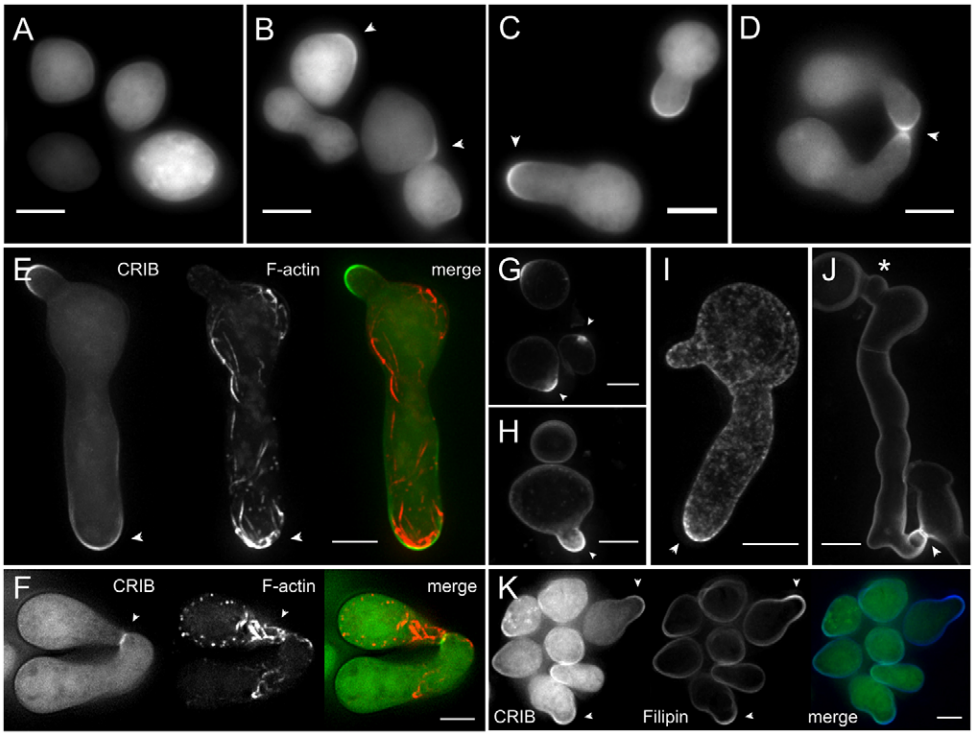

Fig. 5. Colocalization of activated GTPases, F-actin and sterol-rich plasma membrane regions constitute sites of polarized growth. (A) In non-polarized conidia, CRIB fluorescence is evenly distributed in the cytoplasm. (B) Cell symmetry breaking coincides with cortical recruitment of the CRIB reporter, indicating localized activation of Rho GTPases prior to polarized protrusions (arrowheads). (C,D) Crescent-shaped caps of activated GTPases mark the tips of growing germ tubes (C) and CATs (D). See supplementary material Movie 1 for a complete time series of D. (E,F) Co-expression of CRIB–GFP and Lifeact-TagRFP-T shows colocalization of both polarity markers in apical crescents at germ tube tips and CAT fusion sites (arrowheads in E and F, respectively). (G–J) Filipin staining highlights sterol-rich regions (arrowheads) at incipient polarization sites (G), during tip protrusion (H,I) and at newly established CAT fusion sites (J). At older fusion sites, sterol-rich regions have vanished (asterisk in J). (K) Colocalization of filipin-stained sterol-rich plasma membrane regions and the CRIB reporter. Scale bars: 5 μm (A–D, G–J); 4 μm (E,F).

preceded the following change in growth direction. To quantify this temporal sequence further, we developed automated tip-tracking image analysis software (see Materials and Methods). During germ tube avoidance, the apical CRIB crescent shifted in the future growth direction before the actual tip re-orientated (Fig. 6C; supplementary material Movie 4). Quantitative image analysis clearly showed that, over the time course, the peak CRIB fluorescence in the apical crescent of each tip shifted away from the opposing tip during the approach phase, i.e. was off-center in the corresponding heat maps (Fig. 6D), and centered as soon as both tips started to grow away from each other again. The corresponding growth trajectory plots illustrated that the CRIB vector always turned before the tip vector did (Fig. 6E), confirming that activated GTPases move first and tip growth follows. Conversely, in straight growing germ tubes that did not chemotropically interact with other cells, the CRIB reporter was not biased towards a specific side of the tip apex, and consequently the growth trajectory remained fixed in one direction (Fig. 6F–H; supplementary material Movie 5). Taken together, these data demonstrate that repositioning of clusters of locally activated GTPases within the tip apex is consistent with it defining the future growth direction.

RAC-1 is specifically required for CAT formation

Owing to the high similarity to yeast PAKs, and their key function in cell polarization (Kozubowski et al., 2008), CLA-4 and STE-20 of *N. crassa* are believed to interact equally with both CDC-42 and RAC-1 (Bishop and Hall, 2000; Hoffman and Cerione, 2000). Consequently, the CRIB reporters derived from the GTPase-binding regions of these two PAKs label the activated forms of both GTPases. To separate the functional roles of CDC-42 and RAC-1 we used the Rac1 inhibitor NSC23766. This molecule was identified through a structure-based virtual screening of compounds that fit into a surface groove of Rac1 known to be crucial for GEF specification, and which has been shown to specifically block Rac1–GEF interaction *in vitro* and *in vivo* in mammalian cells (Gao et al., 2004). Culturing conidial germlings of *N. crassa* with $\geq$50 μM NSC23766 completely blocked CAT formation and cell fusion, but had no negative effect on germ tube elongation (Fig. 7A–E). By contrast, germ tube elongation was significantly promoted under these conditions (Fig. 7F). Taken together, these data suggest that RAC-1 activity is essential for CAT formation, but dispensable for germ tube growth, which is reminiscent of the Δ*rac-1* germling phenotype (Fig. 2C).

To further verify that NSC23766 was responsible for specific RAC-1 inhibition in *N. crassa*, development of Δ*rac-1* and wild-type germlings was compared in the presence and absence of the inhibitor. No obvious effects on germination and germ tube formation rates, or germ tube morphologies of Δ*rac-1* germlings could be detected, whereas wild-type controls showed the expected changes (Fig. 7G–I). Δ*cdc-42* cells were also included in these experiments; however, owing to the severe polarity defect of this mutant causing extremely slow growth, only

Journal of Cell Science (2014) 127, 1953–1965 doi:10.1242/jcs.141630

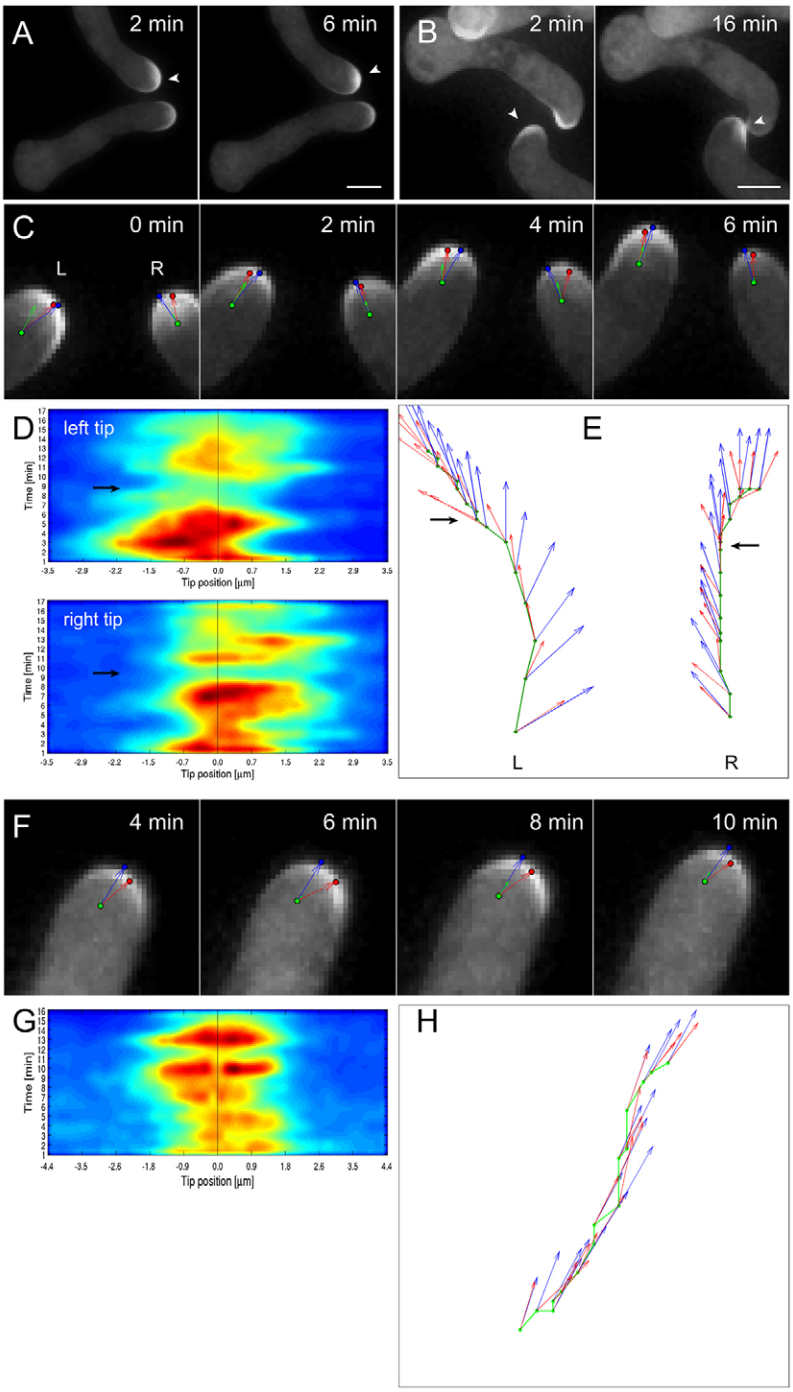

Fig. 6. Lateral displacement of activated Rho GTPases within the tip apex controls directional growth of germ tubes and CATs. (A) During negative chemotropism, the region of maximum CRIB fluorescence (arrowhead) relocated away from the opposing tip. (B) Conversely, during CAT homing, the region of peak CRIB fluorescence (arrowhead) shifted towards the other tip and became focused at the incipient fusion site. Scale bars: 5 µm. (C) During hyphal avoidance responses, lateral displacement of the CRIB signal appeared to take place ahead of substantial changes in growth direction. The tip apex is defined as the point of maximum curvature (blue dot), and thus likely represents the point of maximally targeted secretory vesicle delivery to the apical plasma membrane. Movement of the apex vector (blue vector), therefore indicates a directional change in polarized apex extension. The point of highest GTPase activity within the apical crescent (red dot) is identified as the maximum of a Gaussian fit to the intensity distribution of CRIB reporter fluorescence. Movement of the CRIB vector (red vector) consequently indicates lateral repositioning of activated GTPases within the apical plasma membrane. The overall growth trajectory of the tip is the sum of all displacements of the center of the tip (green dot) from each frame to the next. The length of the tip growth vector (green arrow) thereby indicates the amount of relative tip displacement over time. (D) The complete CRIB distribution un-wrapped along the perimeter of the germ tube apex can be visualized as a heat map to emphasize the transient displacement of the apical crescent from the apex center (vertical black line), particularly to the left at ~3 min for the left tip, and to the right at ~6 min for the right tip. The black arrows indicate a transient drop in localized CRIB fluorescence just after the first turning sequence is completed, shortly after the time of the closest approach. From here, on the left tip, growth switches into a more linear mode as the tips start to grow away from each other, whereas the right tip shows another transient displacement at ~13 min, leading to further bending. (E) The overall growth trajectory of the tip is shown as the displacement of the center of the tip (green dot) over time (green line). The relative movement of tip apex vector (blue arrow) and the CRIB vector (red arrow) from frame to frame, therefore, allows one to determine which of the two tips move first before tip bending occurs. During avoidance, the apex and CRIB vector are not aligned, and the CRIB vector moves in the new growth direction before the apex vector turns. With increasing linear growth apex and CRIB vectors gradually realign. The black arrow corresponds to the arrow in D. (F) Time course showing apical CRIB dynamics in the absence of chemotropic interaction in a straight growing germ tube. (G) Heat map of CRIB reporter fluorescence within the apical crescent over time, showing that the distribution of locally activated GTPases remains well aligned with the tip and apex center. (H) Time plot of automated tip growth analysis. The overall tip growth trajectory (green line) remains fixed in one direction which coincides with apex (blue vectors) and maximal GTPase activity (red vectors) being centrally focused. See supplementary material Movies 2–5 for complete timecourses.

inconclusive data could be obtained within the 6-h incubation period.

Addition of NSC23766 to growing germlings expressing the CRIB reporter led to rapid and permanent dispersal of activated GTPases from CAT tips and arrested cell fusion (Fig. 8A; supplementary material Movie 6). It also led to an immediate decrease (but not complete dispersal) of the CRIB reporter signal from germ tube tips. CRIB reporter crescents in NSC23766-treated germ tube tips usually recovered by 20–30 min after drug addition, and this coincided with the resumption of germ tube elongation (Fig. 8B; supplementary material Movie 7). NSC23766-induced CRIB dispersal also coincided with rapid dissolution of cortical F-actin arrays (Fig. 8C; supplementary material Movie 8). By comparing the localization of fluorescently labeled CDC-42 and RAC-1, we directly confirmed that NSC23766 suppresses cortical localization of RAC-1 but not that of CDC-42 (Fig. 8D,E). Taken together, these findings support the notion that RAC-1 activity is essential for CAT function. NSC23766-mediated inhibitory effects on germ tube growth were only transient, and are probably compensated for through increased recruitment of CDC-42.

Journal of Cell Science (2014) 127, 1953–1965 doi:10.1242/jcs.141630

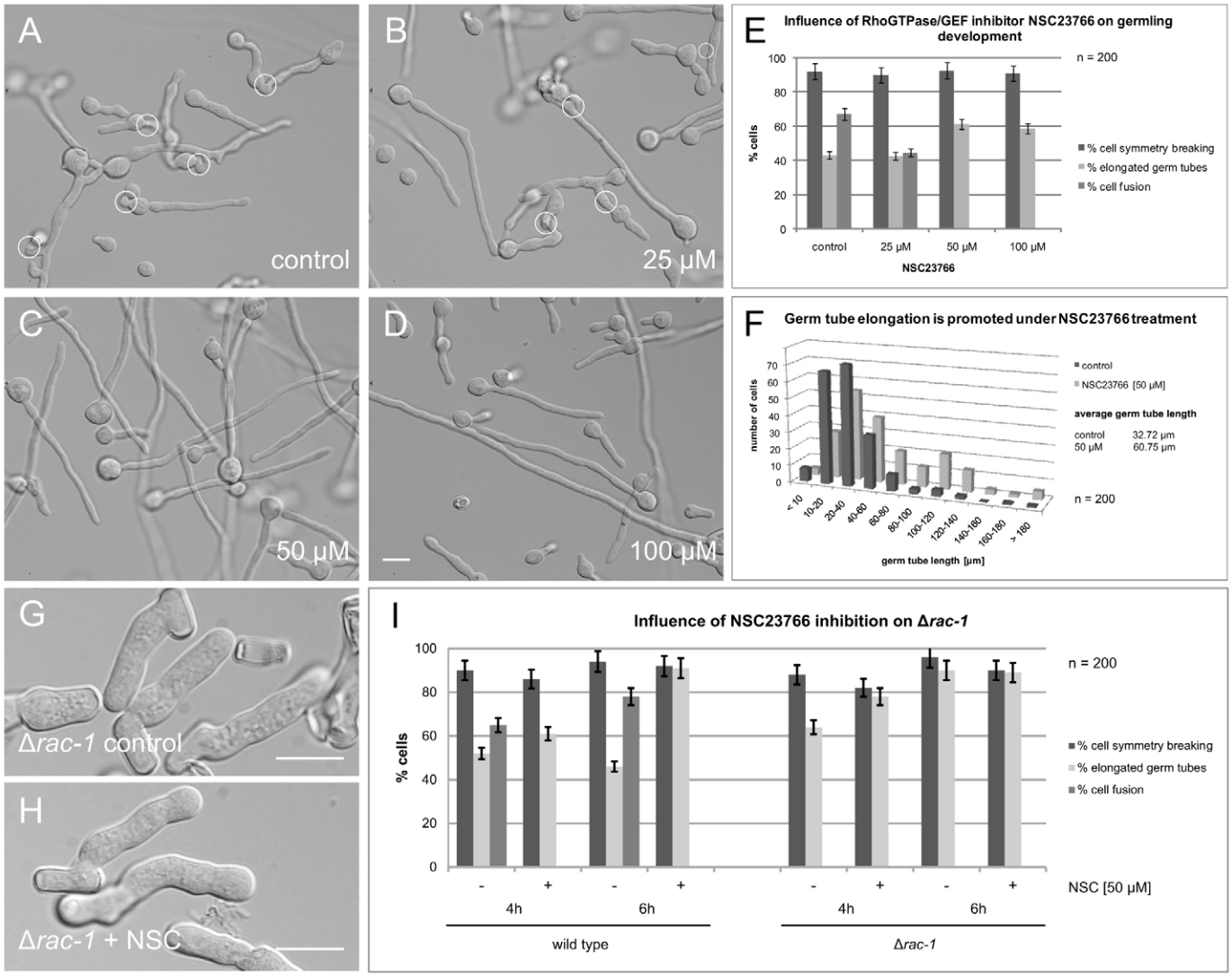

Fig. 7. The Rac1 inhibitor NSC23766 blocks CAT formation and cell fusion specifically and transiently in a concentration-dependent manner. (A–D) Compared to the untreated control, CAT formation and germling fusion is reduced by ~20% in the presence of 25 µM NSC23766 (fusion connections are indicated with circles). In the presence of ≥50 µM of the drug CAT-mediated cell fusion is fully inhibited. (E) Quantification of conidial development under the conditions shown in A–D. (F) Quantification of germ tube development in the presence of 50 µM NSC23766. Compared to the untreated control, the number of cells forming 80–140-µm long germ tubes increases, whereas the number of cells forming 10–60-µm long germ tubes decreases. Overall, this leads to an increase in the average germ tube length by almost a factor of two in the presence of NSC23766. Notably, NSC23766-mediated RAC-1 inhibition is transient. Depending on the starting cell and drug concentration, with time the inhibitory effects of the drug wear off, successively reversing the germling culture back to wild-type morphology. For 50 µM NSC23766 this occurred after about 6 h at 30˚C. (G–I) Addition of NSC23766 showed no obvious morphological effects on germination or germ tube elongation of the Δ*rac-1* mutant, confirming that a RAC-1-specific GEF must be the only target of the inhibitor. Quantifications were performed as explained in detail previously (Lichius et al., 2010; Roca et al., 2010a) and are mean±s.d. Scale bars: 10 µm.

CDC-42 activity is sufficient to drive polarized germ tube growth

In the presence of NSC23766, YFP–CDC-42 became recruited to growing germ tube tips (Fig. 8C), but YFP–RAC-1 did not (Fig. 8D), suggesting that the GTPase activity of CDC-42 was sufficient to drive germ tube elongation in the absence of active RAC-1. Vacuolar accumulation of YFP–RAC-1 increased under the influence of NSC23766 (Fig. 8D), suggesting that RAC-1, when not activated at the apex, quickly became deposited and degraded in vacuoles. These findings support the NSC23766-induced changes in CRIB reporter localization (Fig. 8A,B), and indicate that the drug selectively inhibits RAC-1 and blocks CAT formation and function in *N. crassa*.

RAC-1 inhibition arrests MAK-2 cortical recruitment and oscillation

Oscillatory protein recruitment to CAT tips has recently been recognized as an important regulatory mechanism for self-signaling between genetically identical germlings. The localization of the MAPK MAK-2 has also been found to be predictive of the future growth direction of CATs (Fleißner et al., 2009). Based on our finding that the repositioning of locally activated GTPases within the CAT apex also was a key determinant of tip directionality, we asked whether there is signaling between RAC-1 and MAK-2 during CAT homing. To test this, we challenged chemotropically interacting conidial germlings expressing MAK-2–GFP with the Rac1-inhibitor

Journal of Cell Science (2014) 127, 1953–1965 doi:10.1242/jcs.141630

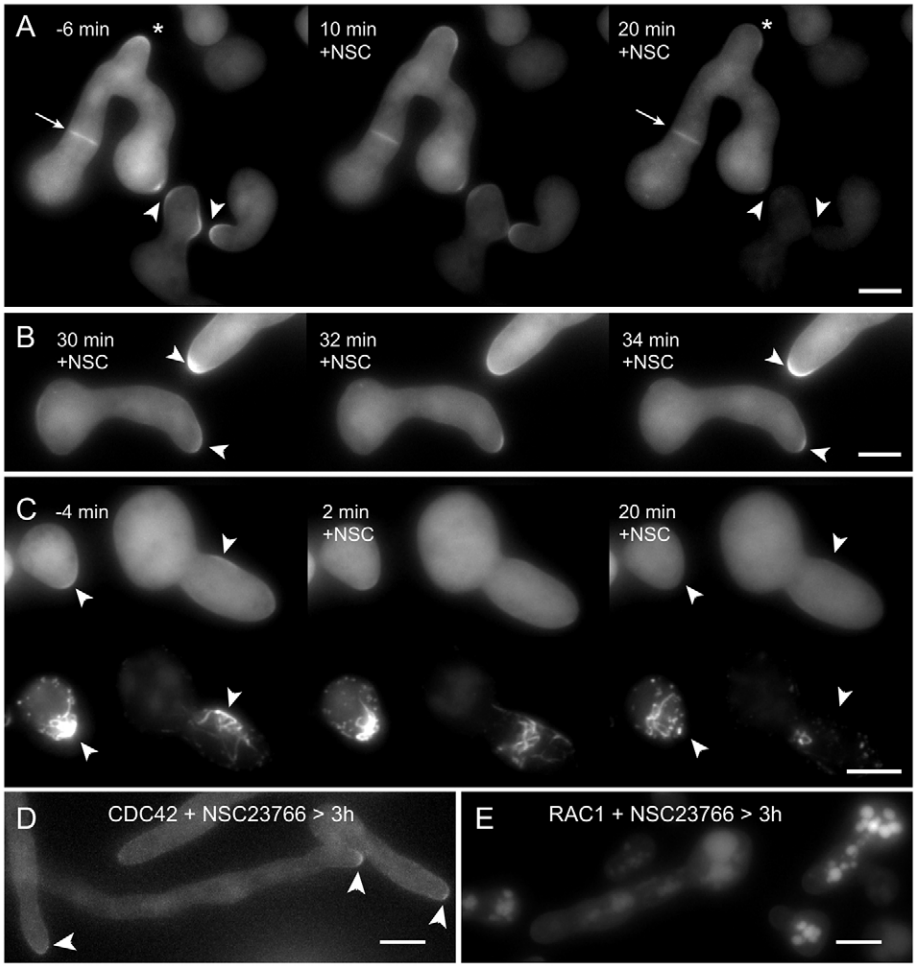

Fig. 8. Inhibition of RAC-1 induces selective and permanent de-activation of GTPases from CAT tips. (A) In the absence of the Rac1 inhibitor NSC23677 (−6 min), activated GTPases are recruited to growing germ tube tips (asterisk), homing CATs (arrowheads) and forming septa (arrow). Upon addition of 100 μM of NSC23766 (10 and 20 min + NSC), the CRIB reporter fluorescence disappears from CATs, weakens but does not completely vanish from germ tube tips, and remains stably associated with septa. (B) In the same slide culture well as shown in A, but 30 min after drug addition, apical crescents of activated GTPase are still functional in growing germ tube tips (arrowheads). (C) NSC23766-induced removal of apically localized, activated GTPases also leads to rapid dispersal of associated F-actin arrays. (D) In the presence of NSC23766, YFP–CDC-42 still localizes to apical crescents at germ tube tips, whereas YFP–RAC-1 is exclusively found inside vacuoles (E). See supplementary material Movies 6–8. Scale bars: 5 μm.

NSC23766. In the absence of the inhibitor, MAK-2 underwent oscillatory recruitment in the form of discrete cortical clusters distributed over the cell body and concentrated at homing and fusing CAT tips (Fig. 9A; supplementary material Movie 9). Addition of NSC23766 initially lengthened the oscillation period; however, eventually MAK-2 fluorescence disappeared completely, and CAT homing and cell fusion were fully arrested (Fig. 9B; supplementary material Movie 10). This evidence indicates that RAC-1 activity is required for the activity and targeted accumulation of MAK-2 into apical clusters at the tips of chemotropically interacting CATs.

DISCUSSION

Conidial germlings of *N. crassa* provide a useful model to study molecular mechanisms of cell polarity regulation and chemotropism that are distinct from those of the yeast paradigm. Genetically identical conidia of *N. crassa* produce germ tubes and CATs that exhibit negative and positive chemotropisms, respectively. We provide evidence that these opposite cell tropisms are regulated by shared and separate functions of the Rho GTPases CDC-42 and RAC-1, with the latter being absent from budding and fission yeasts.

In this study, we established that RAC-1 executes specialized functions during cell fusion in *N. crassa*. Phenotypic analyses of gene deletion mutants showed that CDC-42 is necessary and sufficient for normal germ tube growth, whereas RAC-1 is essential – although not sufficient – for CAT formation. Consequently, the two Rho GTPases are not functionally interchangeable, and the concerted action of both is required for normal germling development in *N. crassa*. In line with previous findings (Araujo-Palomares et al., 2011), a likely scenario for early conidial germling morphogenesis is that CDC-42 establishes polarized growth sites at the cell cortex and, subsequently, additional recruitment of RAC-1 determines CAT formation and function. This was supported by inhibition of CAT formation and cell fusion with the Rac1-specific inhibitor NSC23766, which coincided with active RAC-1 (but not CDC-42) disappearing from the plasma membrane of germ tube tips.

Interestingly, genetic deletion of RAC-1 and its chemical inhibition with NSC23766 did not produce the same germling morphology. Δ*rac-1* germlings displayed a more severe and pleiotropic polarity defect, with shorter and wider germ-tube-like protrusions than NSC23766-mediated RAC-1 inhibition, which resulted in elongated wild-type-like germ tubes. This is consistent with NSC23766 targeting a specific RAC-1–GEF interaction associated with CAT morphogenesis.

In fungi, CRIB reporters have so far been used to investigate polarized growth only in *Saccharomyces cerevisiae* (Ozbudak et al., 2005), *Schizosaccharomyces pombe* (Tatebe et al., 2008; Das et al., 2012) and *Candida albicans* (Corvest et al., 2013). In line with these previous studies, we demonstrated that CRIB reporters derived from *N. crassa* PAKs are robust markers for the discrimination between inactive and active populations of Rho GTPases during polarized growth in filamentous fungi.

Journal of Cell Science (2014) 127, 1953–1965 doi:10.1242/jcs.141630

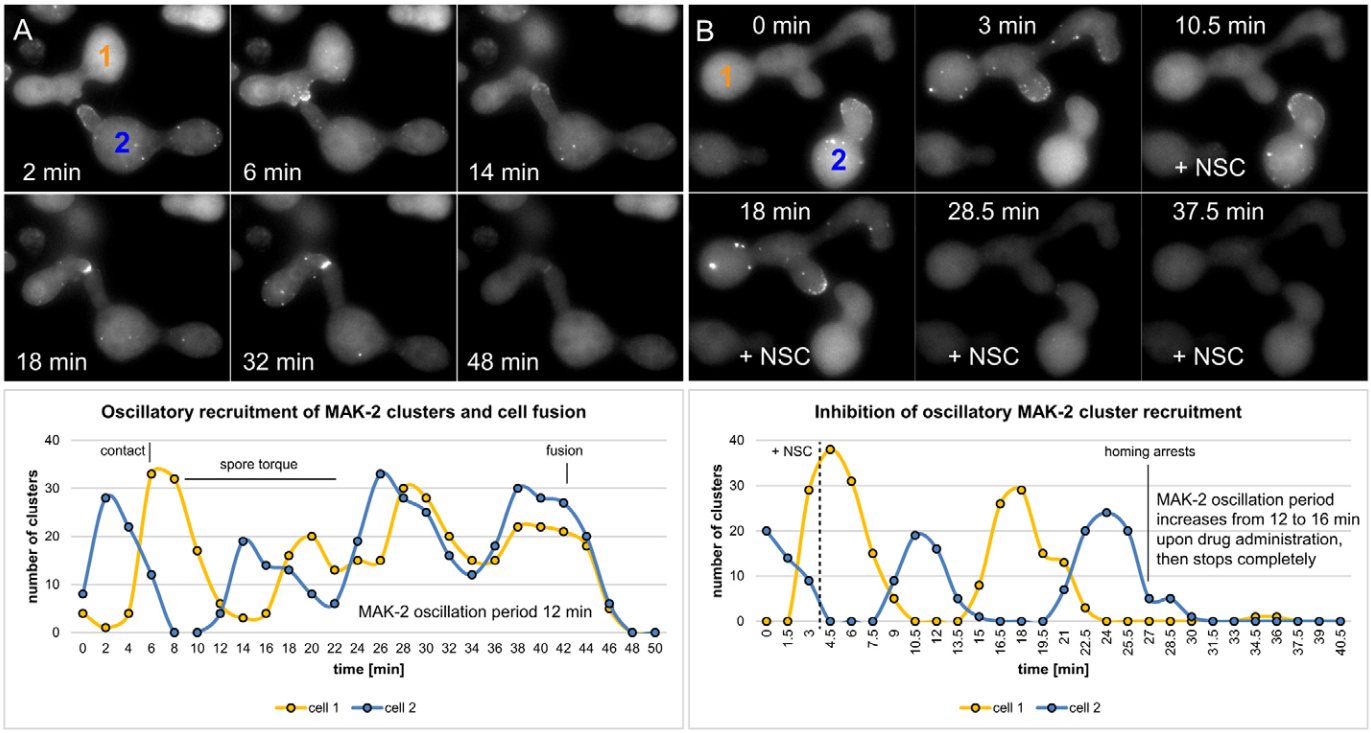

Fig. 9. RAC-1 activity is required for oscillatory recruitment of MAK-2 to CAT tips. Quantitative live-cell imaging analysis of a cortical MAK-2 cluster recruitment during cell fusion in the absence and presence of the Rac1-inhibitor NSC23766. (A) In the control, MAK-2 recruitment occurs as expected with an average oscillation period of ~12 min until cell fusion is completed. 'Spore torque' describes the relative movement of the interacting cells to each other occurring upon contact, and is used here as a clear visual indicator of cell–cell attachment. (B) Addition of NSC23766 during CAT homing leads to an increase in the oscillation period in both cells to ~16 min before cortical recruitment of MAK-2 and CAT homing are fully inhibited. See supplementary material Movies 9, 10.

Colocalization of activated GTPases with F-actin and sterol-rich membrane domains in polarized cell tips strongly suggests that these components constitute a polarity complex that is associated with the cortical plasma membrane and that organizes targeted exocytosis during germ tube and CAT growth.

Underexplored so far is the precise role of both GTPases during septation. Both RAC-1 and CDC-42 have previously been localized to developing septa in conidial germlings and mature hyphae (Araujo-Palomares et al., 2011). Localization of the CRIB reporter confirms that activated GTPases become recruited to these sites. The fact that addition of NSC23766 does not remove the CRIB reporter from septa, furthermore, suggests that CDC-42 takes the primary role in septation. In a previous study, we have shown that the actin-binding protein BUD-6 becomes recruited to the incipient septation site and, together with the formin BNI-1, remains associated with the leading edge of the constricting actomyosin ring (CAR) (Lichius et al., 2012b). It has been suggested that the CDC-42–RAC-1–CDC-24 module acts as a negative regulator of the septation process, counteracting RHO-1 and RHO-4 which have been positively attributed to septation (Rasmussen and Glass, 2005; Rasmussen and Glass, 2007; Justa-Schuch et al., 2010; see also reviews by Seiler and Justa-Schuch, 2010; Mouriño-Pérez and Riquelme, 2013).

Custom-designed tip-tracking software revealed that repositioning of activated GTPases preceded spatial changes of the cell tip growth, and suggested a model by which the lateral displacement of activated GTPase clusters initiates repositioning of the apical secretory vesicle delivery machinery in response to chemotropic cues. This provides an explanation of how directional tip growth is accomplished in germ tubes and CATs that lack a Spitzenkörper.

We furthermore demonstrated that NSC23766-mediated RAC-1 inhibition resulted in the loss of oscillatory MAK-2 recruitment to CAT tips and the cessation of CAT homing. This suggests that during CAT homing the spatio-temporal dynamics of activated Rho-GTPases and membrane-associated MAK-2 clusters are regulated by a feedback mechanism. We also found evidence that CLA-4 – but not STE-20 – is important for CAT formation and cell fusion in *N. crassa*. When considered together, these data indicate that repositioning of activated RAC-1 is probably relayed to MAK-2 via CLA-4. This is consistent with previous work indicating that two separate but complementary GTPase and PAK signaling modules operate in fungi (Li et al., 2004; Mahlert et al., 2006; Rolke and Tudzynski, 2008; Frieser et al., 2011). Recently, BEM-1 has been identified as the likely scaffolding protein for the assembly of a plasma membrane-associated signaling complex capable of interacting with the NRC-1–MEK-2–MAK-2 kinase module during cell fusion (Schürg et al., 2012). The delayed onset and altered morphology of cell fusion that we saw in Δ*cla-4* germlings phenocopies the defects of Δ*bem-1* (Schürg et al., 2012), and supports the hypothesis that BEM-1 and CLA-4 act in the same pathway to regulate CAT formation and function. Dettmann et al. (Dettmann et al., 2012) found evidence that the scaffolding protein HYM-1 has a key role in functionally linking 'ping pong' cell signaling with chemotropic CAT tip growth by acting in two parallel signaling cascades. These dual-use properties of HYM-1 have been linked to phosphorylation of MAK-2 and the physical interaction with both PAKs, STE-20 and

CLA-4 (Dettmann et al., 2012). A ternary Bem1–Rac1–Cla4 complex has also recently been identified to regulate switching between isotropic and polarized growth in *Ustilago maydis* (Frieser et al., 2011).

These cumulative data suggests that a signaling complex comprising the GTPase RAC-1, CDC-24 or another GEF, the scaffolding protein BEM-1 and the PAK CLA-4 is specifically constituted to regulate chemotropic growth of CATs in interaction with the NRC-1–MEK-2–MAK-2 MAPK cascade. We therefore propose that the key function of this interaction is the local assembly of a plasma-membrane-associated active GTPase–PAK–MAPK signaling platform that can regulate chemoattractant perception and secretion, and F-actin nucleation, in order to synchronize oscillatory cell–cell communication and directional CAT tip growth.

MATERIALS AND METHODS

Media and culture conditions

Strains were maintained on solid (2% agar) or in liquid Vogel's minimal medium (VMM) (Vogel, 1956) with 2% sucrose using standard *N. crassa* culture techniques (Davis, 2000). For ignite selection (*bar* resistance gene), NH_4NO_3 was replaced by 0.5% (w/v) proline as an alternative nitrogen source to increase the potency of ignite selection at an effective final concentration of 400 µg/ml (Hays and Selker, 2000). For hygromycin B selection (*hph* resistance gene) (Staben et al., 1989) or nourseothricin selection (*nat1* resistance gene) (Kück and Hoff, 2006), drugs were added after autoclaving at final concentrations of 200 µg/ml and 30 µg/ml, respectively. Development of conidial germlings, including the quantification of CAT-mediated cell fusion, was assessed as described in detail previously (Lichius et al., 2010; Roca et al., 2010a).

Plasmid construction

All plasmids constructed for the heterologous expression of fluorescent fusion proteins were generated using the In-Fusion® PCR cloning system (Clontech, Takara Bio Europe, Saint-Germain-en-Laye, France). For this, a suitable host vector was linearized through restriction enzyme digestion and purified by gel extraction. Coding regions for the promoter, fluorescent protein and protein or protein fragment of interest were amplified either from plasmid DNA or *N. crassa* wild-type genomic DNA or cDNA using specific oligonucleotides extended with 15-bp overhangs compatible to the neighboring 5′ and 3′ fragments comprising the final construct. The purified host vector backbone and up to three individual fragments were joined together in one In-Fusion® *in vitro* recombination reaction prior to transformation into *E. coli*. In-frame cloning of protein coding regions was verified by sequencing. Expression of the fusion constructs was either under control of the glucose-repressible P*ccg-1* promoter (McNally and Free, 1988; Freitag et al., 2004) or the transcription elongation factor-1 promoter (P*tef-1*) (Berepiki et al., 2010; Lichius and Read, 2010).

Strains, transformation and transformant selection

Transformations were performed using a standard electroporation protocol for *N. crassa* as described previously (Margolin et al., 1997). Verified expression plasmids were transformed into wild-type *N. crassa* and gene deletion mutants sourced from the Fungal Genetics Stock Center (FGSC, Kansas City, USA). All strains used and produced in this study are listed in supplementary material Table S1. The homokaryotic status of gene deletion mutants was verified by PCR-genotyping as outlined in detail elsewhere (Lichius et al., 2012a). Transformant strains and expression plasmids generated in this study have been deposited at the FGSC for public use; accession numbers are listed in supplementary material Table S2. Transformants were selected by recovery on either nitrogen-free selection medium containing Ignite (pAL1-CRIB^{CLA-4}) or standard selection medium containing nourseothricin (pAL6-CRIB^{STE-20}, pAL7-CRIB^{CLA-4}, pAL7-CRIB^{STE-20}, pAL11-CRIB^{CLA-4} and pAL11-CRIB^{STE-20}). At least six transformant strains for each construct were screened to show a consistent and unchanged phenotype in comparison to the parental strain after random integration of the fusion construct into the genome. Expression and basic localization of the fusion constructs were verified by fluorescence microscopy in all selected clones, of which ultimately two of each construct were chosen for further investigations.

Live-cell imaging

Conidia were collected from 3- to 5-day-old VMM plate cultures and suspended in sterile water and adjusted to 10^8 cells per ml. In all experiments, unless stated otherwise, conidia were used at a final concentration of 10^6 cells per ml. The cells were incubated in liquid VMM in Lab-Tek 8-well chamber slides (Nalge-Nunc International, Rochester, NY) for 2 to 4 h at 30–35°C and then imaged. Alternatively, to restrict cell movement owing to Brownian motion during 3D and 4D imaging, 8×10^6 cells in aqueous suspension were first evenly spread onto VMM agar in standard Petri dishes using glass beads, then incubated as stated above, and at desired time points 2-cm×2-cm agar squares carrying conidial germlings were prepared using the inverted-agar-block method (Hickey et al., 2005). All imaging experiments were performed as at least three biological replicates. Quantification of germination, germ tube formation and CAT-mediated cell fusion were performed as described in detail previously (Lichius et al., 2010; Roca et al., 2010a).

For differential interference contrast (DIC) microscopy, an inverted Nikon TE2000-U Eclipse widefield microscope (Nikon Instruments Europe BV, UK) equipped with Wollaston polarizer, prism and analyser was used, along with a Nikon Plan Fluor 100×/1.4 NA DIC H oil immersion or Nikon Plan Apo 60×/1.2 NA DIC H water immersion objectives fitted with the corresponding DIC lens sliders. Images were acquired with Nikon ACT-1 software on a Nikon digital DXM1200F color camera and stored as TIFF files.

For widefield epifluorescence microscopy, the same microscope and objectives were used with: a CoolLED *p*E-2 excitation system; a 550 nm LED array module with Nikon G-2A filter for RFP; a 475 nm LED array module with a Nikon B-2A filter for GFP imaging; and a 380 nm LED array module with a Nikon UV-2A for filipin and Calcofluor White (CFW) imaging. Image capture was either with a Hamamatsu Orca-ER C4742-80 camera (Hamamatsu Photonics UK Ltd, Welwyn Garden City, UK) and MetaMorph software v7.7.6.0 (Molecular Devices LLC, Sunnyvale CA, USA,). Optical sectioning was performed with a P-721 PIFOC Z objective focusing system connected to an E-625 PZT piezo servo controller allowing rapid *z*-stack acquisition with 0.2- to 0.5-µm step size. Some time sequences were collected using a Delta-Vision microscope (Applied Precision, Issaquah, WA) consisting of an Olympus IX70 base, an Olympus 100×/1.4 NA Plan-Apo oil immersion objective, a 75-W HBO illuminator; a Chroma Sedat Quad ET filter set (for GFP, excitation 490/20 nm, emission 528/38 nm; for RFP, excitation 545/30 nm, emission 610/75 nm; for FM4-64, excitation 490/20 nm, emission 685/40 nm; for filipin and Calcofluor White, excitation 360/40 nm, emission 457/50 nm; Chroma Technology Corp., Rockingham, VT), a CoolSnap HQ charge-coupled-device (CCD) camera (Photometrics, Tuscon, AZ) and SoftWorx software (AppliedPrecision) for image acquisition. Apart from basic brightness, contrast and display range adjustments using the ImageJ platform (rsbweb.nih.gov/ij/) no further manipulation of the raw data was used to prepare the image files for presentation.

Automated image time course analysis

Tip growth direction and fluorescent reporter protein localization were analyzed using segmentation based on local thresholding and mathematical morphology methods. The developed software has been implemented in a MATLAB environment, and is freely available upon request to: boguslaw.obara@durham.ac.uk. The curvature of the cell boundary was calculated and the boundary point with the highest curvature value used to define the apical position of the tip using an osculating circle. For cells expressing CRIB reporter peptides, the image intensity profiles on the left and right side of the tip position were recorded to provide a map of the plasma membrane protein distribution,

and to determine the relationship between the growth vector and asymmetric CRIB reporter distribution.

Biochemical inhibitors and fluorescent dyes

The water-soluble Rac-specific inhibitor NSC23766 (Gao et al., 2004) (Tocris Bioscience, cat. no. 2161; final concentration 50–200 µM in VMM) was used for the first time in a filamentous fungus to discriminate RAC-specific processes during germling growth and fusion. Filipin III (Sigma cat. no. F4767; final concentration 3–5 µM, 0.1% DMSO) staining was used to visualize accumulations of sterol-rich regions within the plasma membrane. Imaging was restricted to the 5 min following dye addition in order to exclude alteration of membrane structure caused by cytotoxic effects of the dye.

Low-temperature scanning electron microscopy

All samples for low-temperature scanning electron microscopy (LTSEM) were prepared and incubated on VMM agar plates overlaid with sterile cellophane (525-gauge uncoated Rayophane, A.A. Packaging, Preston, UK) to allow rapid sample preparation. At desired time points, ~12-mm^2 cellophane rectangles carrying the specimen were cut out, adhered to the cryospecimen carrier (Gatan, Oxford, UK) with Tissue-Tek OCT compound (Sakura Finetek, Torrance, USA) then immediately cryofixed by plunging into subcooled liquid nitrogen. The specimen carrier was transferred under low vacuum to the cold stage (−120℃) of a 4700II field-emission scanning electron microscope (Hitachi, Wokingham, UK). On the stage, the samples were partially freeze-dried at −80℃ to remove surface ice by sublimation; cooled down to −120℃; sputter-coated in a Gatan Alto 2500 cryopreparation system at −180℃ and coated with ~10 nm of 60:40 gold–palladium alloy (Testbourne Ltd, Basingstoke, UK) in an argon gas atmosphere. The specimen was examined at −160℃ with a beam accelerating voltage of 2 kV, a beam current of 10 µA and working distances of 12–15 mm. Digital images were captured at a resolution of 2560×1920 pixels using, in most cases, the signal from the lower secondary electron detector, and saved as TIFF files.

Acknowledgements

We would like to thank the *Neurospora* Genome Project and the Fungal Genetics Stock Center for continued support in providing *N. crassa* gene deletion mutants. We thank Stephan Seiler (University of Freiburg, Germany) for providing *N. crassa* strains expressing fluorescently labeled GTPases CDC-42 and RAC-1 prior to publication, and acknowledge Junya Shoji (The Samuel Roberts Noble Foundation, USA) for technical help. Special thanks go to Chris E. Jeffree (University of Edinburgh, UK) for invaluable assistance with LTSEM.

Competing interests

The authors declare no competing interests.

Author contributions

A.L. designed and conducted experiments, analysed data and wrote the manuscript. A.B.G. designed experiments, analysed data and wrote the manuscript. M.D.F. designed image analysis software, analysed data and contributed to manuscript writing. B.O. designed image analysis software, analysed data and contributed to manuscript writing. E.C.-L. obtained research funding and contributed to manuscript writing. N.D.R. obtained research funding and contributed to manuscript writing.

Funding

This work was funded by the Biotechnology and Biological Sciences Research Council [grant number BB/E010741/1 to N.D.R.]; SEP-CONACyT [grant number CB2011/169154 to E.C.-L.]; the Human Frontier Science Program [grant number RKP0053/2012 to M.D.F.]; the Royal Society [grant number RG120560 to B.O.]; a School of Biological Sciences (SBS), University of Edinburgh, PhD studentship; and a CONACyT postdoctoral fellowship to A.L.

Supplementary material

Supplementary material available online at
http://jcs.biologists.org/lookup/suppl/doi:10.1242/jcs.141630/-/DC1

References

Adams, A. E., Johnson, D. I., Longnecker, R. M., Sloat, B. F. and Pringle, J. R. (1990). CDC42 and CDC43, two additional genes involved in budding and the establishment of cell polarity in the yeast Saccharomyces cerevisiae. *J. Cell Biol.* **111**, 131-142.

Araujo-Palomares, C. L., Castro-Longoria, E. and Riquelme, M. (2007). Ontogeny of the Spitzenkörper in germlings of Neurospora crassa. *Fungal Genet. Biol.* **44**, 492-503.

Araujo-Palomares, C. L., Richthammer, C., Seiler, S. and Castro-Longoria, E. (2011). Functional characterization and cellular dynamics of the CDC-42-RAC-CDC-24 module in Neurospora crassa. *PLoS ONE* **6**, e27148.

Bartnicki-Garcia, S., Bartnicki, D. D., Gierz, G., López-Franco, R. and Bracker, C. E. (1995). Evidence that Spitzenkörper behavior determines the shape of a fungal hypha: a test of the hyphoid model. *Exp. Mycol.* **19**, 153-159.

Berepiki, A., Lichius, A., Shoji, J. Y., Tilsner, J. and Read, N. D. (2010). F-actin dynamics in Neurospora crassa. *Eukaryot. Cell* **9**, 547-557.

Bernards, A. and Settleman, J. (2004). GAP control: regulating the regulators of small GTPases. *Trends Cell Biol.* **14**, 377-385.

Bishop, A. L. and Hall, A. (2000). Rho GTPases and their effector proteins. *Biochem. J.* **348**, 241-255.

Borkovich, K. A., Alex, L. A., Yarden, O., Freitag, M., Turner, G. E., Read, N. D., Seiler, S., Bell-Pedersen, D., Paietta, J., Plesofsky, N. et al. (2004). Lessons from the genome sequence of Neurospora crassa: tracing the path from genomic blueprint to multicellular organism. *Microbiol. Mol. Biol. Rev.* **68**, 1-108.

Brand, A. and Gow, N. A. R. (2009). Mechanisms of hypha orientation of fungi. *Curr. Opin. Microbiol.* **12**, 350-357.

Chen, R. E. and Thorner, J. (2007). Function and regulation in MAPK signaling pathways: lessons learned from the yeast Saccharomyces cerevisiae. *Biochim. Biophys. Acta* **1773**, 1311-1340.

Corvest, V., Bogliolo, S., Follette, P., Arkowitz, R. A. and Bassilana, M. (2013). Spatiotemporal regulation of Rho1 and Cdc42 activity during Candida albicans filamentous growth. *Mol. Microbiol.* **89**, 626-648.

Das, M., Drake, T., Wiley, D. J., Buchwald, P., Vavylonis, D. and Verde, F. (2012). Oscillatory dynamics of Cdc42 GTPase in the control of polarized growth. *Science* **337**, 239-243.

Davis, R. H. (2000). *Neurospora: Contributions of a Model Organism*. Oxford: Oxford University Press.

Dettmann, A., Illgen, J., März, S., Schürg, T., Fleissner, A. and Seiler, S. (2012). The NDR kinase scaffold HYM1/MO25 is essential for MAK2 map kinase signaling in Neurospora crassa. *PLoS Genet.* **8**, e1002950.

Fleissner, A., Leeder, A. C., Roca, M. G., Read, N. D. and Glass, N. L. (2009). Oscillatory recruitment of signaling proteins to cell tips promotes coordinated behavior during cell fusion. *Proc. Natl. Acad. Sci. USA* **106**, 19387-19392.

Freitag, M., Hickey, P. C., Raju, N. B., Selker, E. U. and Read, N. D. (2004). GFP as a tool to analyze the organization, dynamics and function of nuclei and microtubules in Neurospora crassa. *Fungal Genet. Biol.* **41**, 897-910.

Frieser, S. H., Hlubek, A., Sandrock, B. and Bolker, M. (2011). Cla4 kinase triggers destruction of the Rac1-GEF Cdc24 during polarized growth in Ustilago maydis. *Mol. Biol. Cell.* **22**, 3253-3262.

Gao, Y., Xing, J., Streuli, M., Leto, T. L. and Zheng, Y. (2001). Trp(56) of rac1 specifies interaction with a subset of guanine nucleotide exchange factors. *J. Biol. Chem.* **276**, 47530-47541.

Gao, Y., Dickerson, J. B., Guo, F., Zheng, J. and Zheng, Y. (2004). Rational design and characterization of a Rac GTPase-specific small molecule inhibitor. *Proc. Natl. Acad. Sci. USA* **101**, 7618-7623.

Goryachev, A. B. and Pokhilko, A. V. (2008). Dynamics of Cdc42 network embodies a Turing-type mechanism of yeast cell polarity. *FEBS Lett.* **582**, 1437-1443.

Hays, S. and Selker, E. U. (2000). Making the selectable marker bar tighter and more economical. *Fungal Genet. Newslett.* **47**, 107.

Hickey, P. C., Jacobson, D., Read, N. D. and Louise Glass, N. L. (2002). Live-cell imaging of vegetative hyphal fusion in Neurospora crassa. *Fungal Genet. Biol.* **37**, 109-119.

Hickey, P. C., Swift, S. R., Roca, M. G. and Read, N. D. (2005). Live-cell Imaging of filamentous fungi using vital fluorescent dyes and confocal microscopy. In *Methods in Microbiology*, Vol. 34, pp. 63-87. Elsevier.

Hoffman, G. R. and Cerione, R. A. (2000). Flipping the switch: the structural basis for signaling through the CRIB motif. *Cell* **102**, 403-406.

Jaffe, A. B. and Hall, A. (2005). Rho GTPases: biochemistry and biology. *Annu. Rev. Cell Dev. Biol.* **21**, 247-269.

Justa-Schuch, D., Heilig, Y., Richthammer, C. and Seiler, S. (2010). Septum formation is regulated by the RHO4-specific exchange factors BUD3 and RGF3 and by the landmark protein BUD4 in Neurospora crassa. *Mol. Microbiol.* **76**, 220-235.

Karnoub, A. E., Worthylake, D. K., Rossman, K. L., Pruitt, W. M., Campbell, S. L., Sondek, J. and Der, C. J. (2001). Molecular basis for Rac1 recognition by guanine nucleotide exchange factors. *Nat. Struct. Biol.* **8**, 1037-1041.

Kozubowski, L., Saito, K., Johnson, J. M., Howell, A. S., Zyla, T. R. and Lew, D. J. (2008). Symmetry-breaking polarization driven by a Cdc42p GEF-PAK complex. *Curr. Biol.* **18**, 1719-1726.

Kück, U. and Hoff, B. (2006). Application of the nourseothricin acetyltransferase gene (*nat1*) as dominant marker for transformation of filamentous fungi. *Fungal Genet. Newsl.* **53**, 9-11.

Kulkarni, K., Yang, J., Zhang, Z. and Barford, D. (2011). Multiple factors confer specific Cdc42 and Rac protein activation by dedicator of cytokinesis (DOCK) nucleotide exchange factors. *J. Biol. Chem.* **286**, 25341-25351.

Lengeler, K. B., Davidson, R. C., D'souza, C., Harashima, T., Shen, W.-C., Wang, P., Pan, X., Waugh, M. and Heitman, J. (2000). Signal transduction

cascades regulating fungal development and virulence. *Microbiol. Mol. Biol. Rev.* **64**, 746-785.
Li, L., Xue, C., Bruno, K., Nishimura, M. and Xu, J. R. (2004). Two PAK kinase genes, CHM1 and MST20, have distinct functions in Magnaporthe grisea. *Mol. Plant Microbe Interact.* **17**, 547-556.
Li, D., Bobrowicz, P., Wilkinson, H. H. and Ebbole, D. J. (2005). A mitogen-activated protein kinase pathway essential for mating and contributing to vegetative growth in Neurospora crassa. *Genetics* **170**, 1091-1104.
Lichius, A. and Read, N. D. (2010). A versatile set of Lifeact-RFP expression plasmids for live-cell imaging of F-actin in filamentous fungi. *Fungal Genetics Report* **57**, 8-14.
Lichius, A., Roca, M. G. and Read, N. D. (2010). How to distinguish conidial anastomosis tubes (CATs) from germ tubes. *The Neurospora Protocol Guide*, 1-6.
Lichius, A., Lord, K. M., Jeffree, C. E., Oborny, R., Boonyarungsrit, P. and Read, N. D. (2012a). Importance of MAP kinases during protoperithecial morphogenesis in Neurospora crassa. *PLoS ONE* **7**, e42565.
Lichius, A., Yáñez-Gutiérrez, M. E., Read, N. D. and Castro-Longoria, E. (2012b). Comparative live-cell imaging analyses of SPA-2, BUD-6 and BNI-1 in Neurospora crassa reveal novel features of the filamentous fungal polarisome. *PLoS ONE* **7**, e30372.
Lopez-Franco, R. and Bracker, C. E. (1996). Diversity and dynamics of the Spitzenkörper in growing hyphal tips of higher fungi. *Protoplasma* **195**, 90-111.
Maerz, S., Ziv, C., Vogt, N., Helmstaedt, K., Cohen, N., Gorovits, R., Yarden, O. and Seiler, S. (2008). The nuclear Dbf2-related kinase COT1 and the mitogen-activated protein kinases MAK1 and MAK2 genetically interact to regulate filamentous growth, hyphal fusion and sexual development in Neurospora crassa. *Genetics* **179**, 1313-1325.
Mahlert, M., Leveleki, L., Hlubek, A., Sandrock, B. and Bölker, M. (2006). Rac1 and Cdc42 regulate hyphal growth and cytokinesis in the dimorphic fungus Ustilago maydis. *Mol. Microbiol.* **59**, 567-578.
Margolin, B. S., Freitag, M. and Selker, E. U. (1997). Improved plasmids for gene targeting at the his-3 locus of Neurospora crassa by electroporation. *Fungal Genet. Newsl.* **44**, 34-36.
McNally, M. T. and Free, S. J. (1988). Isolation and characterization of a Neurospora glucose-repressible gene. *Curr. Genet.* **14**, 545-551.
Mercker, M., Kollath-Leiss, K., Allgaier, S., Weiland, N. and Kempken, F. (2009). The BEM46-like protein appears to be essential for hyphal development upon ascospore germination in Neurospora crassa and is targeted to the endoplasmic reticulum. *Curr. Genet.* **55**, 151-161.
Miller, P. J. and Johnson, D. I. (1994). Cdc42p GTPase is involved in controlling polarized cell growth in Schizosaccharomyces pombe. *Mol. Cell. Biol.* **14**, 1075-1083.
Mouriño-Pérez, R. R. and Riquelme, M. (2013). Recent advances in septum biogenesis in Neurospora crassa. *Adv. Genet.* **83**, 99-134.
Nelson, W. J. (2003). Adaptation of core mechanisms to generate cell polarity. *Nature* **422**, 766-774.
Ozbudak, E. M., Becskei, A. and van Oudenaarden, A. (2005). A system of counteracting feedback loops regulates Cdc42p activity during spontaneous cell polarization. *Dev. Cell* **9**, 565-571.
Pandey, A., Roca, M. G., Read, N. D. and Glass, N. L. (2004). Role of a mitogen-activated protein kinase pathway during conidial germination and hyphal fusion in Neurospora crassa. *Eukaryot. Cell* **3**, 348-358.
Rasmussen, C. G. and Glass, N. L. (2005). A Rho-type GTPase, rho-4, is required for septation in Neurospora crassa. *Eukaryot. Cell* **4**, 1913-1925.
Rasmussen, C. G. and Glass, N. L. (2007). Localization of RHO-4 indicates differential regulation of conidial versus vegetative septation in the filamentous fungus Neurospora crassa. *Eukaryot. Cell* **6**, 1097-1107.
Read, N. D., Goryachev, A. B. and Lichius, A. (2012). The mechanistic basis of self-fusion between conidial anastomosis tubes during fungal colony initiation. *Fungal Biol. Rev.* **26**, 1-11.
Roca, M. G., Arlt, J., Jeffree, C. E. and Read, N. D. (2005). Cell biology of conidial anastomosis tubes in Neurospora crassa. *Eukaryot. Cell* **4**, 911-919.
Roca, M. G., Lichius, A. and Read, N. D. (2010a). How to analyze and quantify conidial anastomosis tube (CAT)-mediated cell fusion. *The Neurospora Protocol Guide*, 1-3.
Roca, M. G., Kuo, H.-C., Lichius, A., Freitag, M. and Read, N. D. (2010b). Nuclear dynamics, mitosis, and the cytoskeleton during the early stages of colony initiation in Neurospora crassa. *Eukaryot. Cell* **9**, 1171-1183.
Rolke, Y. and Tudzynski, P. (2008). The small GTPase Rac and the p21-activated kinase Cla4 in Claviceps purpurea: interaction and impact on polarity, development and pathogenicity. *Mol. Microbiol.* **68**, 405-423.
Schmidt, A. and Hall, A. (2002). Guanine nucleotide exchange factors for Rho GTPases: turning on the switch. *Genes Dev.* **16**, 1587-1609.
Schürg, T., Brandt, U., Adis, C. and Fleissner, A. (2012). The Saccharomyces cerevisiae BEM1 homologue in Neurospora crassa promotes co-ordinated cell behaviour resulting in cell fusion. *Mol. Microbiol.* **86**, 349-366.
Seabra, M. C. and Wasmeier, C. (2004). Controlling the location and activation of Rab GTPases. *Curr. Opin. Cell Biol.* **16**, 451-457.
Seiler, S. and Justa-Schuch, D. (2010). Conserved components, but distinct mechanisms for the placement and assembly of the cell division machinery in unicellular and filamentous ascomycetes. *Mol. Microbiol.* **78**, 1058-1076.
Staben, C., Jensen, B., Singer, M., Pollock, J., Schechtman, M., Kinsey, J. and Selker, E. U. (1989). Use of a bacterial Hygromycin B resistance gene as a dominant selectable marker in Neurospora crassa transformation. *Fungal Genetics Newsl.* **36**, 79-81.
Takahashi, S. and Pryciak, P. M. (2007). Identification of novel membrane-binding domains in multiple yeast Cdc42 effectors. *Mol. Biol. Cell* **18**, 4945-4956.
Takeshita, N., Higashitsuji, Y., Konzack, S. and Fischer, R. (2008). Apical sterol-rich membranes are essential for localizing cell end markers that determine growth directionality in the filamentous fungus Aspergillus nidulans. *Mol. Biol. Cell* **19**, 339-351.
Tatebe, H., Nakano, K., Maximo, R. and Shiozaki, K. (2008). Pom1 DYRK regulates localization of the Rga4 GAP to ensure bipolar activation of Cdc42 in fission yeast. *Curr. Biol.* **18**, 322-330.
Virag, A., Lee, M. P., Si, H. and Harris, S. D. (2007). Regulation of hyphal morphogenesis by cdc42 and rac1 homologues in Aspergillus nidulans. *Mol. Microbiol.* **66**, 1579-1596.
Vogel, H. J. (1956). A convenient growth medium for Neurospora (Medium N). *Microbiol. Genet. Bull.***13**, 42-43.

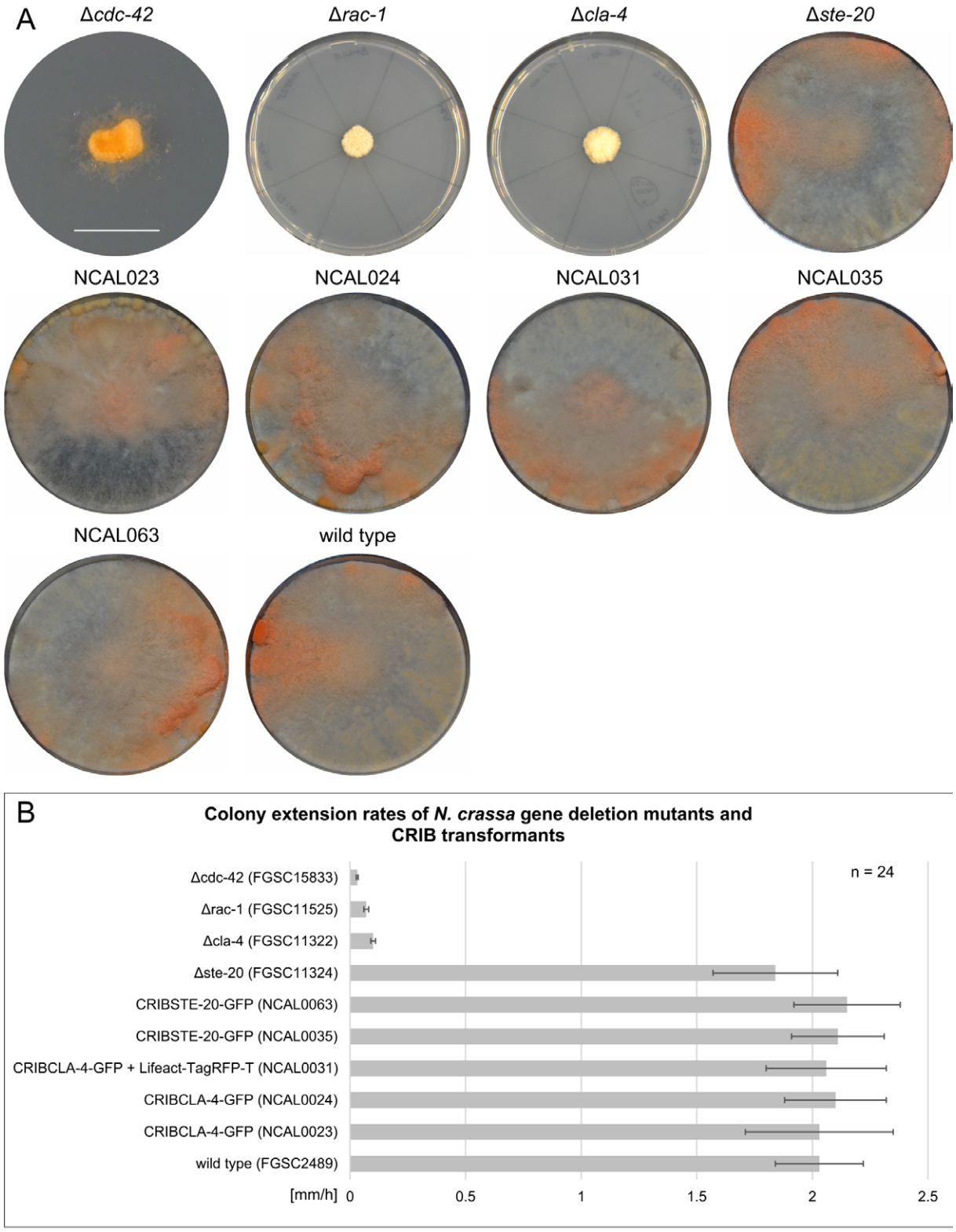

Fig. S1. Phenotypic evaluation of gene deletion mutants and CRIB transformants. (A) Δ*ste-20* is the only strain of the four gene deletion mutants used in this study that did not display a severe polarized growth defect. All transformants expressing CRIB reporter constructs developed normal colony growth indistinguishable from the wild type control. Except Δ*cdc-42* which was grown for 10 days, all other strains have been incubated for 3 days at 30°C in the light. Scale bar, 10 mm. All other images show the full Petri culture dishes with ~ 8.5 cm diameter. **(B)** Colony extension measurements of the cultures shown in (A). The three polarized growth mutants Δ*cdc-42*, Δ*rac-1* and Δ*cla-4*, show as expected significantly reduced colony extension rates of below 0.1 mm/h. Apart from Δste-20 which shows a slightly reduced mean colony extension rate of 1.84 mm/h, all CRIB transformant strains grow as quickly as the wild type with mean colony extension rates between 2.03-2.15 mm/h. Mean colony extension rates were calculated from growth distances along eight radii on each plate measured in three three-hour intervals after an initial over-night incubation of the colony. For each strain duplicate plates were used. Error bars indicate standard deviations.

Movie 1. Time course of Figure 5*D* showing recruitment of activated GTPases labelled with the CRIB reporter into apical crescents at homing CAT tips. Upon CAT contact, fluorescence concentrates at the attachment site and disappears upon completion of the fusion pore. Opening of the fusion pore is visible as a gradually increasing gap at the fusion site.

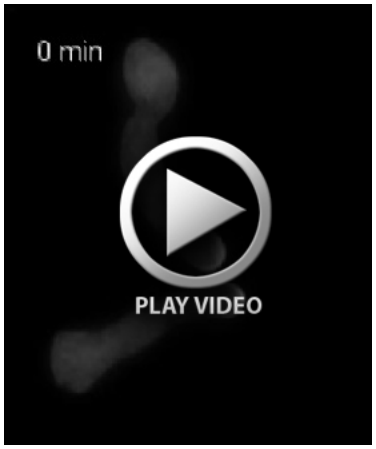

Movie 2. Time course of Figure 6*A* showing CRIB reporter dynamics in the tip apices of avoiding germ tubes. The peak CRIB reporter fluorescence becomes gradually moved away from the opposing tip.

Movie 3. Time course of Figure 6*B* showing CRIB reporter dynamics in the tip apices during germling fusion. The peak CRIB reporter fluorescence becomes gradually moved towards the opposing tip.

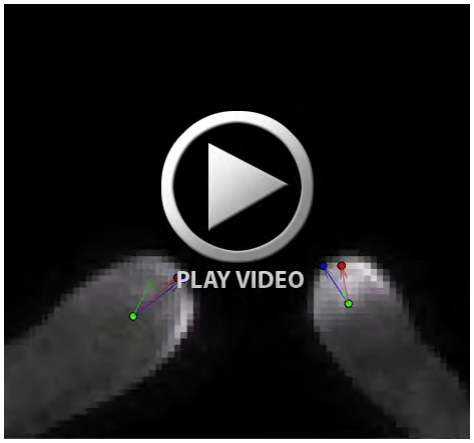

Movie 4. Time course of Figure 6*C* showing the result of automated image analysis assigning apex center and apex vector (blue dot and arrow), CRIB peak intensity and CRIB vector (red dot and vector), and tip center and tip growth vector (green dot and arrow), during germ tube avoidance.

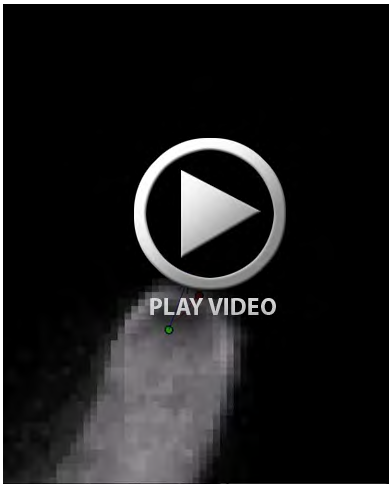

Movie 5. Time course of Figure 6*F* showing the result of automated image analysis during straight germ tube growth in the absence of chemotropic interaction.

Movie 6. Time course of Figure 8*A* showing the inhibitory effect of the Rac1-inhibitor NSC23766 on cortical recruitment of activated GTPases labelled with the CRIB reporter. Shortly upon NSC23766 addition apical crescents of CRIB rapidly disappear from germ tube and CAT tips indicating that membrane-associated activation of GTPases is blocked. Removal of activated GTPases coincides with the arrest of polarized cortex protrusion.

Movie 7. Image sequence of Figure 8*B* showing that apical recruitment of activated GTPases to germ tube tips reestablishes after some time despite the presence of the Rac1-inhbitor and can drive polarized tip protrusion.

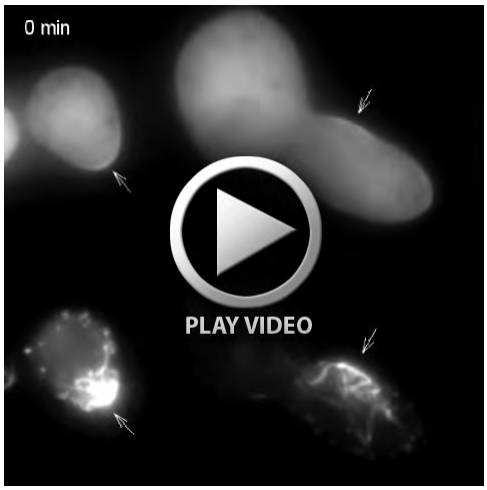

Movie 8. Time course of Figure 8*C* showing cells co-expressing the CRIB reporter and the F-actin marker Lifeact-TagRFP-T demonstrating that removal of activated GTPases from the cell cortex by NSC23766 treatment coincides with the dissolution of associated F-actin arrays.

Movie 9. Time course of Figure 9*A* showing oscillatory recruitment of MAK-2 into cortical clusters distributed over the cell body and concentrated at CAT tips and cell fusion sites. Physical attachment of both cells is evident by the spore torque response, i.e. the relative movement of both cells to each other during establishment of contact and opening of the fusion pore. Upon successful fusion, oscillations stop and MAK-2 fluorescence quickly disappears from the fusion site.

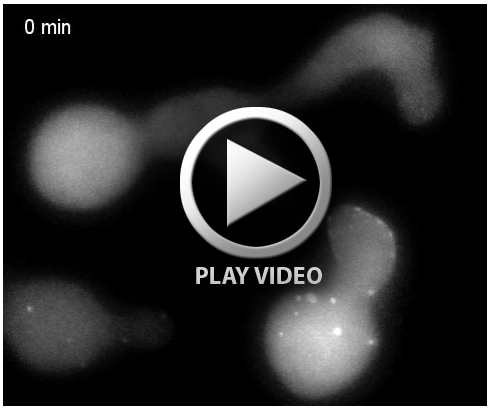

Movie 10. Time course of Figure 9*B* showing the inhibitory effect of the Rac1-inhibitor NSC23766 on cortical recruitment of MAK-2. Shortly after the addition of NSC23766 MAK-2 oscillations slow down and eventually cease, coinciding with homing arrest and the inhibition of cell fusion.

Table S1. *Neurospora crassa* strains used and produced in this study.

Strain	***Genotype***	***Source***
wild type	*74-OR23-1VA, mat A*	*FGSC2489
wild type	*ORS-SL6a, mat a*	FGSC4200
Δ*cla-4*	Δ*cla4::hph*$^{+}$*, mat a* (homokaryon)	FGSC11322
Δ*ste-20*	Δ*ste20::hph*$^{+}$*, mat A* (homokaryon)	FGSC11324
Δ*rac-1*	Δ*rac1::hph*$^{+}$*, mat a* (heterokaryon)	FGSC11495
Δ*rac-1*	Δ*rac-1::hph*$^{+}$*, mat a* (homokaryon after single spore isolation on selection medium)	this study
Δ*rac-1*	Δ*rac-1::hph*$^{+}$*, mat a* (homokaryon)	FGSC11525
Δ*cdc-42*	Δ*cdc42::hph*$^{+}$*, mat a* (homokaryon)	FGSC15833
wt CRIB^{CLA-4}-GFP	*Pccg1::crib^{cla-4}-gfp::bar*$^{+}$*, mat a*	this study
wt CRIB^{CLA-4}-GFP	*Pccg1:: crib^{cla-4}-gfp::bar*$^{+}$*, mat A*	this study
wt sCRIB-GFP	*Pccg1::scrib-gfp::bar*$^{+}$*, mat a*	this study
wt CRIB^{CLA-4}-GFP + Lifeact-TagRFP	*Pccg1::crib^{cla-4}-gfp::bar*$^{+}$*, Pccg1::lifeact-tagrfp::bar*$^{+}$, mat A	this study
wt CRIB^{CLA-4}-GFP + Lifeact-TagRFP-T	*Pccg1::crib^{cla-4}-gfp::bar*$^{+}$*, Pccg1::lifeact-tagrfp-t::bar*$^{+}$, mat A	this study
wt CRIB^{STE-20}-TagRFP-T	*Pccg1::crib^{ste-20}-tagrfp-t::nat1*$^{+}$, mat a	this study
wt CRIB^{STE-20}-TagRFP-T	*Pccg1::crib^{ste-20}-tagrfp-t::nat1*$^{+}$, mat A	this study
wt CRIB^{STE-20}-GFP	*Pccg1::crib^{ste-20}-gfp::nat1*$^{+}$, mat a	this study
wt CRIB^{CLA-4}-GFP	*Pccg1::crib^{cla-4}-gfp::nat1*$^{+}$, mat a	this study
wt MAK-2-GFP	*Pccg1::mak-2-gfp::nat1*$^{+}$, mat a	(Lichius *et al*., 2012a)
Δ*mak-2* MAK-2-GFP	*Pccg-1::mak-2-gfp::nat1*$^{+}$, mat a	(Lichius *et al*., 2012a)
YFP-CDC42	*Pgpd::yfp-cdc42::his-3, Δcdc-42::hph*$^{+}$*, mat a*	(Araujo-Palomares et al., 2011)
YFP-RAC1	*Pgpd::yfp-rac1::his-3, Δrac::hph*$^{+}$*, mat a*	(Araujo-Palomares et al., 2011)

*FGSC (Fungal Genetics Stock Center)

Table S2. *Neurospora crassa* transformant strains and expression plasmids deposited at the Fungal Genetics Stock Center (FGSC).

FGSC #	***Strain***	***Genotype***
10774	wt CRIB^{CLA-4}-GFP	*Pccg1::crib^{cla-4}-gfp::bar^{+}, mat a*
10775	wt CRIB^{CLA-4}-GFP	*Pccg1:: crib^{cla-4}-gfp::bar^{+}, mat A*
10776	wt sCRIB-GFP	*Pccg1::scrib-gfp::bar^{+}, mat a*
10777	wt CRIB^{CLA-4}-GFP + Lifeact-TagRFP	*Pccg1::crib^{cla-4}-gfp::bar^{+},* *Pccg1::lifeact-tagrfp::bar^{+}*, mat A
10778	wt CRIB^{CLA-4}-GFP + Lifeact-TagRFP-T	*Pccg1::crib^{cla-4}-gfp::bar^{+},* *Pccg1::lifeact-tagrfp-t::bar^{+}*, mat A
10779	wt CRIB^{STE-20}-TagRFP-T	*Pccg1::crib^{ste-20}-tagrfp-t::nat1^{+}*, mat a
10780	wt CRIB^{STE-20}-TagRFP-T	*Pccg1::crib^{ste-20}-tagrfp-t::nat1^{+}*, mat A
10781	wt CRIB^{STE-20}-GFP	*Pccg1::crib^{ste-20}-gfp::nat1^{+}*, mat a
10782	wt CRIB^{CLA-4}-GFP	*Pccg1::crib^{cla-4}-gfp::nat1^{+}*, mat a
10783	wt CRIB^{CLA-4}-GFP	*Ptef-1::CRIB^{CLA-4}-GFP::nat1*, mat a
10784	wt CRIB^{STE-20}-GFP	*Ptef-1::CRIB^{STE-20}-GFP::nat1*, mat A
Plasmid #	***Plasmid***	***Genotype***
833	pAL1-CRIB^{CLA-4}	*Pccg1::crib^{cla-4}-gfp::bar^{+}*
834	pAL1-sCRIB	*Pccg1::scrib-gfp::bar^{+}*
835	pAL6-CRIB^{STE-20}	*Pccg-1::CRIB^{STE-20}-TagRFP-T::nat1*
836	pAL7-CRIB^{STE-20}	*Pccg-1::CRIB^{STE-20}-GFP::nat1*
837	pAL7-CRIB^{CLA-4}	*Pccg-1::CRIB^{CLA-4}-GFP::nat1*
838	pAL11-CRIB^{CLA-4}	*Ptef-1::CRIB^{CLA-4}-GFP::nat1*
839	pAL11-CRIB^{STE-20}	*Ptef-1::CRIB^{STE-20}-GFP::nat1*